The American Journal of Pathology, Vol. 193, No. 4, April 2023

ELSEVIER

The American Journal of PATHOLOGY

ajp.amjpathol.org

VASCULAR BIOLOGY, ATHEROSCLEROSIS, AND ENDOTHELIUM BIOLOGY

Endothelial Glycocalyx and Cardiomyocyte Damage Is Prevented by Recombinant Syndecan-1 in Acute Myocardial Infarction

Carl Vahldieck,[*†] Eleonora Cianflone,[‡] Benedikt Fels,[*§] Samuel Löning,[*] Patrik Depelmann,[*] Jolanda Sabatino,[‡¶‖] Nadia Salerno,[‡] Christian M. Karsten,[**] Daniele Torella,[††] Joachim Weil,[‡‡] Dong Sun,[§§] Michael S. Goligorsky,[§§] and Kristina Kusche-Vihrog[*§]

From the Institute of Physiology, the Department of Anesthesiology and Intensive Care Medicine,† University Medical Centre Schleswig-Holstein Campus Luebeck, and the Institute for Systemic Inflammation Research,** University of Luebeck, Luebeck, Germany; the Departments of Medical and Surgical Sciences‡ and Experimental and Clinical Medicine,†† University Magna Græcia of Catanzaro, Catanzaro, Italy; DZHK (German Research Centre for Cardiovascular Research),§ Partner Site Hamburg/Luebeck/Kiel, Luebeck, Germany; the Division of Pediatric Cardiology,¶ Department of Women's and Children's Health, University Hospital Padua, Padua, Italy; the Pediatric Research Institute "Città della Speranza",‖ Padua, Italy; Medizinische Klinik II,‡‡ Sana Kliniken Luebeck, Luebeck, Germany; and the Renal Research Institute and Departments of Medicine, Pharmacology and Physiology,§§ New York Medical College, Valhalla, New York*

Accepted for publication December 20, 2022.

Address correspondence to Carl Vahldieck, M.D., Institute of Physiology, University of Luebeck, Ratzeburger Allee 160, 23562 Luebeck, Germany. E-mail: carl.vahldieck@uksh.de.

The outer layer of endothelial cells (ECs), consisting of the endothelial glycocalyx (eGC) and the cortex (CTX), provides a protective barrier against vascular diseases. Structural and functional impairments of their mechanical properties are recognized as hallmarks of endothelial dysfunction and can lead to cardiovascular events, such as acute myocardial infarction (AMI). This study investigated the effects of AMI on endothelial nanomechanics and function and the use of exogenous recombinant syndecan-1 (rSyn-1), a major component of the eGC, as recovering agent. ECs were exposed *in vitro* to serum samples collected from patients with AMI. In addition, *in situ* ECs of *ex vivo* aorta preparations derived from a mouse model for AMI were employed. Effects were quantified by using atomic force microscopy—based nanoindentation measurements, fluorescence staining, and histologic examination of the mouse hearts. AMI serum samples damaged eGC/CTX and augmented monocyte adhesion to the endothelial surface. In particular, the anaphylatoxins C3a and C5a played an important role in these processes. The impairment of endothelial function could be prevented by rSyn-1 treatment. In the mouse model of myocardial infarction, pretreatment with rSyn-1 alleviated eGC/CTX deterioration and reduced cardiomyocyte damage in histologic analyses. However, echocardiographic measurements did not indicate a functional benefit. These results provide new insights into the underlying mechanisms of AMI-induced endothelial dysfunction and perspectives for future studies on the benefit of rSyn-1 in post-AMI treatment. *(Am J Pathol 2023, 193: 474–492; https://doi.org/10.1016/j.ajpath.2022.12.009)*

Ischemic heart disease (IHD) is the single most common cause of death worldwide. Indeed, the frequency of IHD is increasing, and the associated mortality is close to 10% during hospitalization.[1] Despite improvements in the treatment of IHD, acute myocardial infarction (AMI) remains one of the most common life-threatening events in industrialized countries.[2] To further improve outcomes of patients with AMI, it is imperative to design new strategies and therapeutic approaches.[3]

Supported by a German Cardiac Society research grant (C.V.); Deutsche Forschungsgemeinschaft grants KU1496/7-1, KU1496/7-3, and INST392/141-1 (K.K.-V.); NIH grant HL144528 (D.S. and M.S.G.); and New York Community Trust research and educational grant (M.S.G.).

Disclosures: None declared.

https://doi.org/10.1016/j.ajpath.2022.12.009

Acute ischemic events, such as AMI, often cause cardiogenic shock, characterized by acute hypotension resulting in global tissue hypoxia with subsequent organ failure.[4,5] AMI immediately activates the sympathoadrenal system with an excessive increase in circulating catecholamines,[5] immunogenic factors such as ILs,[6] the complement system,[7] and acute-phase proteins such as C-reactive protein[8] or matrix metalloproteinases (MMPs),[6] leading to injury of the heart and vasculature.[6,9–11] Pathophysiological changes include microcirculatory dysfunction with vascular leakage, edema, and an increase in leukocyte and platelet adhesion to the endothelium.[10,12] In general, ischemic injury is one of the most prominent clinical condition characterized by endothelial activation or damage.[4,5,13] Notably, endothelial damage in ischemia (eg, shock) may be both generalized and localized to selective organs, such as the heart, kidney, lung, or liver.[13] Endothelial cells (ECs), especially endothelial glycocalyx (eGC), together with the underlying endothelial cortex (CTX), have been recognized as central modulators of the pathophysiological processes during acute ischemic events, such as AMI,[2,4,13,14] and targeting them may open new therapeutic approaches for IHD.[9,13,15]

Together, the eGC and the CTX establish a vasoprotective nanobarrier of the vascular system.[16,17] More importantly, the eGC covers the luminal endothelial surface and consists of a variety of carbohydrate-rich molecules such as glycoproteins, proteoglycans, glycosaminoglycans, and associated plasma proteins.[18,19] The glycosaminoglycans include heparan sulfate, chondroitin sulfate, and hyaluronic acid, and they are attached to transmembrane syndecans and membrane-bound glypicans.[18] Syndecan-1 (Syn-1; CD138) is a transmembrane proteoglycan that builds the structural backbone of the eGC.[20] It acts as a core unit for other eGC components and transmits extracellular signals to the intracellular environment through its transmembrane domain, which is directly associated with the actin cytoskeleton of the CTX.[20,21]

The CTX is an actin-rich layer, located 50 to 150 nm underneath the plasma membrane.[18,22] Its nanomechanical properties (such as stiffness) inversely correlate with endothelial nitric oxide (NO) release: increased stiffness of the cell cortex induces a decrease in NO production and vice versa.[22,23] Together, the eGC and CTX form a responsive hub. Their nanomechanical properties, such as stiffness and height,[18,22] are highly flexible and can be most reliably probed using atomic force microscopy (AFM). Concerning the nanomechanical properties of eGC, a flat and soft conformation indicates shedding of eGC components.[18] Interaction between eGC and CTX enables coordinated reactions to a large number of stimuli from the bloodstream.[16,17] Damage to either eGC or CTX mutually influences their nanomechanical properties, thereby affecting endothelial functions.[24] Thus, changes in the nanomechanical properties of eGC or CTX contribute to decreased NO production[25] and can be seen as hallmarks for endothelial dysfunction and pathologic vascular conditions.[22]

Structural damage to the eGC can also be detected during AMI by increasing plasma levels of its principal constituents Syn-1 and heparan sulfate.[4,5,13] Furthermore, increased serum-soluble Syn-1 constitutes an independent predictor of short-term mortality in patients with acute heart disease.[2] In acute or critical settings, such as in AMI, accelerated restoration of the eGC may thus determine the clinical outcome of patients.[15] During AMI, activation of the complement system is an early marker of inflammation and tissue injury.[7] The anaphylatoxins C3a and C5 play a pathophysiological role for myocardial ischemia and reperfusion injury.[26] Furthermore, complement activation promotes inflammation and shedding of the glycocalyx in renal ischemia and reperfusion injury.[27]

In this context, a promising approach to expeditiously restoring the eGC involves treating ECs either with liposomal nanocarriers of preassembled glycocalyx or single components of the eGC, such as Syn-1, as previously reported.[15] Considering the prominent role of Syn-1 for eGC integrity and endothelial signaling function, we hypothesized that treatment with exogenous recombinant full-length Syn-1 (rSyn-1) protects against AMI-induced vascular and cardiac damage. To test this hypothesis, ECs were treated *in vitro* and *ex vivo* as well as in mice after myocardial infarction (MI) *in vivo* with recombinant full-length Syn-1, and the nanomechanical properties of the eGC and CTX were analyzed in an AFM-based model. The present data underline the feasibility of accelerated eGC restoration with Syn-1 and amelioration of myocardial injury after MI.

Materials and Methods

Cell Isolation and Culture

Umbilical cords were donated by patients giving birth in the Marien-Krankenhaus Luebeck (approved by Local Ethics Committee Case: 18-325). To isolate the ECs from the umbilical cord vein, the umbilical cord was washed several times with phosphate-buffered saline (PBS). After cleansing the cord, 10 to 15 mL of 1 mg/mL dispase (Gibco, Carlsbad, CA) was injected in the umbilical vein and incubated for 1 hour at 37°C to cleave fibronectin and collagen IV, thereby exposing the ECs by degrading the extracellular matrix. The resulting solution, including human umbilical vein endothelial cells (HUVECs), was centrifuged at 129 × *g* for 10 minutes. The supernatant was aspirated, and the cell pellet was resuspended in HUVEC culture medium [Gibco Medium 199 + fetal calf serum 10% (Gibco) + penicillin/streptomycin 1% (Gibco; 100 U/mL; 100 mg/mL) + Large Vessel Endothelia Supplement 1% (Gibco) + heparin, 5000 U/mL (Biochrom, Schaffhausen, Switzerland)]. The cell solution

was then transferred to a gelatin-coated culture flask [gelatin 0.5% (Sigma Aldrich, St. Louis, MO)] and cultivated in the incubator at 37°C, 21% O_2 and 5% CO_2. Cells from six different umbilical cords were isolated, pooled, split into several cryotubes, and frozen in liquid nitrogen for storage. Cells were used up to the second passage.

Enzymatic removal of eGC components: stimulation with heparinase-I (Hep-I; 0.1 U/μL) for 60 minutes, followed by a 24-hour recovery period either with or without rSyn-1 (8 pmol/L for 24 hours).

Serum stimulation of ECs: stimulation with 10% patient (AMI) or healthy donor [control (CTR)] serum (instead of fetal calf serum) for 24 hours either with or without rSyn-1 (8 pmol/L for 24 hours).

Synthesis of Full-Length Syndecan-1

In all commercially available syndecan-1 products, the N-termini are truncated and lack the transmembrane and intracellular domains. Such a truncation impedes its incorporation into lipid bilayers. For this reason, a recombinant full-length syndecan-1 was generated.

Steps for expression and purification of this transmembrane protein are as follows:

i) Transient transfection of HEK293 cells (mammalian expression system is preferable to preserve protein glycosylation).
ii) The complete coding sequence of the protein.

Amino acid sequence of recombinant mouse Syn-1 protein expressed:

MRRAALWLWLCALALRLQPALPQIVAVNVPPEDQ DGSGDDSDNFSGSGTGALPDTLSRQTPSTWKDVWLL TATPTAPEPTSSNTETAFTSVLPAGEKPEEGEPVLHVE AEPGFTARDKEKEVTTRPRETVQLPITQRASTVRVT TAQAAVTSHPHGGMQPGLHETSAPTAPGQPDHQPPR VEGGGTSVIKEVVEDGTANQLPAGEGSGEQDFTFETS GENTAVAAVEPGLRNQPPVDEGATGASQSLLDRKEVL GGVIAGGLVGLIFAVCLVAFMLYRMKKKDEGSYSLEE PKQANGGAYQKPTKQEEFYATRTRPLEDYKDDDDK GSHHHHHH.

iii) Recombinant protein was prepared from cell lysate, which was made with a modified radioimmunoprecipitation assay lysis buffer (25 mmol/L Tris-HCl, pH 7.4, 150 mmol/L NaCl, 1% Nonidet P-40, 1 mmol/L EDTA, 1× protein inhibitor cocktail mix, and 1 mmol/L phenylmethylsulfonyl fluoride).
iv) The volume used for each lane in the SDS-PAGE was 20 μL sample + 3 μL reducing reagent + 7.5 μL of sample buffer.
v) The purity of protein isolation was confirmed using SDS-PAGE by detecting a single band of predicted size of the glycosylated form of syndecan-1, as shown in Supplemental Figure S1.

Fluorescence Staining and Microscopy

HUVECs were fixed with either 4% paraformaldehyde or 0.1% glutaraldehyde for 30 minutes for further staining. Afterwards, the coverslips were washed three times with PBS (+/+) and stored at 4°C in the dark until staining.

Cortical F-actin was stained using phalloidin-tetramethylrhodamine (Sigma Aldrich). After fixation with glutaraldehyde, the cells were permeabilized for 10 minutes in 0.1% Triton X-100 (Sigma Aldrich; catalog number T8787-50ML), blocked for 30 minutes with 10% normal goat serum, and incubated for 60 minutes with phalloidin-tetramethylrhodamine (10 μg/mL) in normal goat serum (darkness, room temperature). After several washes in PBS (+/+), the coverslips were mounted overnight at 4°C with Dako mounting medium (Dako, Carpinteria, CA) containing Hoechst (Sigma Aldrich; 1.5 μg/mL).

Wheat germ agglutinin (WGA; conjugate Alexa-Fluor-488; Thermo Fisher, Waltham, MA) was used as overview staining for eGC components. The glutaraldehyde-fixated cells were carefully washed with PBS (+/+) and then incubated with 1:500 dilutions of WGA (conjugate Alexa-Fluor-488) in PBS (+/+) for 1 hour at room temperature in a wet chamber in the dark. After incubation, the coverslips were carefully washed three to five times for 5 minutes with PBS (+/+) on a belly dancer (set to slowest movement) and mounted overnight, as described above.

For immunostaining of syndecan-1 (CD138), fixed HUVECs were blocked for 30 minutes with 10% normal goat serum and incubated with the primary antibody (mouse anti-human CD138; monoclonal antibody; Bio-Rad, Hercules, CA; 1:100; catalog number MCA2459). After incubation, the coverslips were washed carefully in PBS (+/+) and incubated with the secondary antibody (goat anti-mouse conjugate Alexa-488; Invitrogen, Carlsbad, CA) 1:400 in normal goat serum for 60 minutes. Coverslips were mounted with Dako mounting medium containing Hoechst (1.5 μg/mL).

Images were rendered with a Keyence fluorescence microscope BZ9000 (Keyence Corp., Osaka, Japan; magnification ×60) using the BZ Viewer/Analyzer-II software version 2.2; Keyence Corp.). Images and stacks of WGA and phalloidin stainings were analyzed for fluorescence intensity using ImageJ software version 1.52a; NIH, Bethesda, MD; https://imagej.nih.gov/ij/download.html, last accessed October 10, 2022). For analyzing the amount of syndecan-1 per cell, fluorescence-dot nuclei colocalization was measured using YT Evaluation software version 2.1.12014 (64 bit; Synentec, Elmshorn, Germany). Each staining process was repeated four to six times, processing 25 to 30 recordings per coverslip for statistical analysis.

Quantification of Soluble Syndecan-1

A soluble syndecan-1 (CD138) enzyme-linked immunosorbent assay (ELISA; Diaclone Research, Cedex, France;

catalog number 950.640.192) was used to quantitatively determine levels of syndecan-1 in the culture medium of stimulated monolayers or patient serum samples. After stimulation, the conditioned medium was collected and stored according to the manufacturer's instructions. Soluble syndecan-1 was measured by adding conditioned medium or serum samples to the solid-phase sandwich ELISA.

Patients

Blood samples of patients with AMI were collected from January to April 2020 at the University of Luebeck (Luebeck, Germany) in cooperation with the Department of Cardiology and Angiology of the "Sana Kliniken Luebeck" Hospital (Luebeck, Germany), in accordance with the Declaration of Helsinki and approved by the Local Ethics Committee (case: 19-310). Samples were collected from female and male patients, aged 48 to 85 years (mean ± SD age: 65 ± 11.8 years) who were admitted to the hospital with the diagnosis of acute coronary syndrome manifesting as AMI (hereafter termed AMI group). Only patients with ST-elevation MI who received a percutaneous coronary intervention as first-line therapy during the first 120 minutes after diagnosis of ST-elevation MI were included. A second blood sample was collected 3 days after AMI from the same patients (hereafter termed AMI-d3 group). Patients who underwent cardiopulmonary resuscitation or after gaining a return of spontaneous circulation were excluded, as were patients who died during or after percutaneous coronary intervention.

Patients with AMI were enrolled randomly after obtaining written informed consent ($N = 10$). Healthy age- and sex-matched volunteers without cardiovascular comorbidities served as controls (hereafter termed CTR group). Serum samples from patients and controls were immediately treated according to the recommended assessment of individual complement components in whole blood by Brandwijk et al.[28] Therefore, samples were kept on ice and centrifuged at 4°C within 60 minutes after collection. After pooling, the samples were snap frozen and stored at −80°C.

Monocyte Adhesion Measurements

Monocytes were isolated from the blood of healthy donors using the S-pluriBead Maxi Reagent Kit (pluriSelect Life Science, Leipzig, Germany; catalog number 70-50010-12) following the manufacturer's instructions. For quantification of monocyte adhesion, isolated human monocytes were fluorescently labeled with an Alexa Flour 488 anti-human CD14 antibody (Biolegend, San Diego, CA; catalogue number 367130) and added to the HUVEC monolayer for 4 hours. To remove nonadherent monocytes, cells were washed carefully four times with PBS, following a standardized protocol. HUVECs and adherent monocytes were fixed with 4% paraformaldehyde and subjected to fluorescence microscopy for further analysis.

Adhesion force measurements were performed by using the Nanowizard4 CellHesion-Module (JPK BioAFM Business, Berlin, Germany) equipped with a petri dish heater for maintaining 37°C, as recently described.[29] Briefly, arrow TL-2 tipless cantilevers (NanoAndMore GmbH, Wetzlar, Germany) were incubated before all experiments for 20 minutes in Corning Cell-Tak (Fisher Scientific GmbH, Schwerte, Germany; catalog number 10317081) to attach an isolated human monocyte to the tipless cantilever. To quantify the adhesion forces, the monocyte was brought into contact with the endothelial surface for 10 seconds with a constant set point of 0.5 V. Force-distance curves were obtained by probing HUVEC monolayers with a monocyte-carrying cantilever. Maximal adhesion forces between monocyte and endothelial surface were measured and analyzed using the JPK Data processing software version 7.0.112 (Bruker Nano GmbH, Berlin, Germany). Throughout the whole procedure, the EC layer was always covered by HEPES-buffered saline.

Complement Receptor Antagonists and Quantification of Complement Anaphylatoxins

The anaphylatoxins C3a and C5a were quantified from the serum of patients with AMI using ELISA (Thermo Fisher Scientific, Hamburg, Germany; C3a, catalog number BMS2089; C5a, catalog number RAB0631). Serum samples with high levels of anaphylatoxins were used to stimulate HUVECs, as described above.

Specific receptor antagonism to C3a-receptor-1 was achieved by applying SB-290157 (Sigma Aldrich; catalog number 559410) and C5a-receptor-1 using PMX53 (Sigma Aldrich; catalog number 533683), according to the manufacturer's instructions (both: concentration 1:1000/24 hours).

Mouse MI Model

Animals

All animal experimental procedures were approved by Magna Græcia Institutional Review Boards on Animal Use and Welfare and performed according to the *Guide for the Care and Use of Laboratory Animals*[30] from directive 2010/63/EU of the European Parliament. All animals received humane care, and all efforts were made to minimize animal suffering. Mice were housed under controlled conditions of 25°C, 50% relative humidity, and a 12-hour light (6 AM to 6 PM) and 12-hour dark cycle, with water and food (containing 18.5% protein) available ad libitum. Mice were anesthetized by intraperitoneally injecting tiletamine/zolazepam (80 mg/kg) or inhaling isoflurane (isoflurane 1.5% and oxygen 98.5%; Iso-Vet; Chanelle Pharma, Galway, Ireland). As wild-type animals, 8-week−old C57BL/6J female mice were used (Jackson Laboratory, Bar Harbor, ME; stock number 000664).

Echocardiography

Before echocardiography, mice were anesthetized with isoflurane. Unconscious mice were weighed and secured in a supine position on a temperature-controlled restraining board. Anesthesia was maintained with 1% to 2% isoflurane in oxygen delivered through a nose cone. Four-limb lead electrocardiograms (Vevo 3100 and MP150; Biopac, Goleta, CA) were simultaneously recorded. All hair in the thoracic region was removed using a depilatory agent, and the area was cleansed with water. Ultrasound gel was applied to the thoracic region to improve sound wave transmission. In all mice, heart rates were maintained at >400 beats per minute while images were being recorded. Echocardiographic images were obtained with a Vevo 3100 system (Visualsonics, Inc., Toronto, ON, Canada) equipped with an MX550D ultra–high-frequency linear array transducer (22 to 55 MHz). The transducer was positioned in a stationary stand perpendicular to the mouse (in some cases, manual adaptations were needed for optimal imaging). In brief, a frame rate of >200 frames per minute was maintained for all B- and M-mode images. B-mode long-axis parasternal images were recorded when optimal views of the aorta, papillary muscle, and endocardium were visible. M-mode short-axis images were recorded at the level of the papillary muscles, and the left ventricle (LV) was bisected to obtain the optimal M-mode selection. Conventional echocardiographic measurements of the LV included ejection fraction, fractional shortening, end-diastolic dimension, end-systolic dimension, anterior and posterior wall thickness, and mass. For long-axis B-mode measurements, the endocardium was traced semi-automatically beginning from the mitral valve and excluding the papillary muscle. Ejection fraction and fractional shortening were calculated by computer using standard computational methods. Speckle-tracking echocardiography was used for advanced cardiac analysis (regional and global cardiac measurements; Vevo LAB analysis software version v3.2.0; FUJIFILM VisualSonics, Toronto, ON, Canada). Cardiac cycles were acquired digitally from the parasternal long-axis and midventricular short-axis views to assess radial, circumferential, and longitudinal systolic strain/velocity (in accordance with myocardial fiber orientation at varying levels of the LV wall) and time-to-peak systolic strain/velocity. Images selected for strain analysis had well-defined endocardial and epicardial borders and no substantial image artifacts. Image analysis was performed according to the manufacturer's instructions. The endocardium and epicardium were traced semi-automatically using VevoStrain software version v2.1.0 (FUJIFILM VisualSonics). The traces were manually adjusted to ensure adequate tracking of endocardial and epicardial borders. Velocity, displacement, strain, and strain rate were calculated for radial and longitudinal planes. In the long axis, the basal anterior septum, middle anterior septum, apical anterior septum, basal posterior wall, middle posterior wall, and apical posterior segments were defined. In the midventricular short axis, the anterior, anterior septum, inferior septum, inferior, posterior, and anterior-lateral segments were further delineated. Tissue contraction patterns were expressed as negative strain values for longitudinal and circumferential motion and positive values for radial strain. In each segment, peak systolic strain (percentage) and time to peak systolic strain (milliseconds) were analyzed. Global average peak values for circumferential and longitudinal strain are reported.

MI Procedure

The MI procedure was performed on 8-week–old C57BL/6J female mice (body weight, 20 to 25 g) through permanent ligation of the left anterior descending coronary artery, as previously described.[29,31] Briefly, animals were intubated with a 22-gauge tube, ventilated with a mechanical ventilator (28026 mouse ventilator; Ugo Basile, Gemonio, Italy; tidal volume, 0.2 mL; 120 strokes/minute), and anesthetized with inhaled isoflurane, maintaining a body temperature of 37°C ± 2°C. The fourth intercostal space was opened to expose the heart. A 7.0 silk suture was passed under the left anterior descending coronary artery and tied to occlude the vessel. The pneumothorax was then reduced, the chest was sutured, and the animals were allowed to recover. Postsurgical analgesia was achieved by administering buprenorphine (0.1 mg/kg), and ampicillin, 150 mg/kg, was given at the end of surgery. The animals were divided into different groups based on the experimental arm: control group (saline i.v. injection, sham operated); syndecan-1 group (i.v. injection of syndecan-1 at a final concentration of 4 μg/mouse 24 hours before sham operation); MI group (i.v. saline injection); and MI + syndecan-1 group (i.v. injection of syndecan-1 at final concentration of 4 μg/mouse 24 hours before MI). Animals were sacrificed 9 days after MI or the sham operation procedure. Acute mortality rate within 24 hours after MI procedure was overall approximately 20%.

For the glycocalyx measurements, syndecan-1 was dissolved at a concentration of 5 mg/mL in 1× PBS. The dose and route of administration was 4 μg/mouse intravenously. Syndecan-1 was injected 24 hours before the MI procedure.

Cardiac Troponin Analysis

To assess the presence of myocyte necrosis induced by the experimental procedure, the levels of high-sensitive cardiac troponin T in the blood serum were analyzed 9 days after MI. Animals were anesthetized, and 1 mL of blood was taken from the orbital sinus by inserting the tip of a fine-glass Pasteur pipette into the corner of the eye underneath the eyeball, directing the tip at a 45-degree angle toward the middle of the eye. The blood was collected in a vacutainer (Vacuette Tube 3 mL K3E K3EDTA; number 454086; Greiner Bio-One GmbH, Frickenhausen, Germany). The threshold for cardiac troponin T positivity in mice was established at the 99th percentile of cardiac troponin T values in blood samples from 15 consecutive control mice, using a commercially available and clinically validated cardiac troponin T blood kit.[32]

Tissue Harvesting

Aorta and heart samples were collected 9 days after MI. For harvesting aorta and heart, the animals were anesthetized, the chest was opened, the diaphragm was excised, and the abdominal aorta was cannulated to wash heart and aorta with 1× PBS. The first 1.5 to 2 cm of the aorta was harvested. After removing blood and carefully cleansing the heart and the aorta, organs were transferred to a transportation solution (Solution 8) and kept at 4°C until further processing.[33]

Atomic Force Microscopy

The thickness and stiffness of eGC and the stiffness of CTX in both HUVECs and mouse aortic ECs were determined using the AFM nano-indentation technique, as described previously.[34–36] Indentation measurements were performed on living confluent ECs (HUVECs) at 37°C using a Nanoscope Multimode8 AFM (Veeco, Mannheim, Germany). For measuring *ex vivo* aortas, a Nanowizard4 (JPK BioAFM Business, Berlin, Germany) was employed.

The central component of the AFM is a triangular cantilever with a mounted spherical tip (diameter = 10 μm; Novascan, Ames, IA), which is a sensitive mechanical nanosensor. This cantilever is used to periodically indent the cells and functions as a soft spring with a spring constant of 10 pN/nm (for eGC) or 30 pN/nm (for CTX). A laser beam is targeted at the gold-coated back side of the cantilever and reflected to a position-sensitive quadrupled photodiode so that the cantilever deflection (V) can be quantified. To help calculate the force (F) acting on the cantilever and, in turn, the force exerted by the cantilever on the sample, the authors determined the spring constant of the cantilever (Kcant) in advance using the thermal tuning method and the deflection sensitivity (α) of the cantilever on bare glass coverslips ($F = V \times \alpha \times Kcant$). Knowing both the piezo displacement (xpiezo) and the deflection sensitivity (α), the indentation depth (deformation) of the sample (xsample) can be calculated [$xsample = xpiezo - (\alpha \times V)$]. In the following, the indentation depth is called thickness. Plotting the force (F) necessary to indent a single cell (thickness, xsample) gives force indentation curves. The sample stiffness can be derived from Hooke's law (Ksample = F/xsample). The stiffness (K) is the sample's mechanical resistance against a defined deformation (eg, indentation) and is strongly determined by the indentation depth and its location because of the varying distribution of cellular organelles. The experimental parameters were as follows: indentation velocity, 1 μm/second; loading force, approximately 500 pN (for eGC) or 3 nN (for cortex); indentation frequency, 0.5 Hz; and ramp size, 2 μm; these parameters lead to a trigger threshold of 50 nm (for eGC) or 100 nm (for CTX).

All experiments were performed in HEPES-buffered solution (standard composition in mmol/L: 140 NaCl, 5 KCl, 1 $MgCl_2$, 1 $CaCl_2$, 5 glucoses, and 10 HEPES, pH 7.4) supplemented with 1% fetal calf serum to prevent eGC collapse.

From each preparation (cell samples or *ex vivo* aortas), the stiffness of $N = 5$ to 6 (repetitions/aorta) with $n = 150$ to 300 (ECs per sample) was determined; six to eight force distance curves were generated for each cell and averaged. Force distance curve data were collected with the following: i) Research NanoScope version 9.20 (64 bit; Bruker Nano GmbH) or ii) Nanowizard4 XP control software version 7.0.119 (Bruker Nano GmbH) or iii) JPK Data processing software version 7.0.112 (Bruker Nano GmbH). Stiffness values were calculated from force distance curves using the protein unfolding and nanoindentation analysis software Punias 3D version 1.0 (release 2.3; *http://punias.free.fr/punias3.html?q=pages/download_of_software*).

Preparation of Mouse Aortas/Assessment of Mouse Aortic Endothelial Cell Nanomechanics

The aortas were harvested and prepared for *ex vivo* analysis by AFM, as described previously,[34–36] to assess the thickness and stiffness of the eGC and CTX of the mouse aorta ECs. Briefly, aortas were harvested after sacrificing the animals and freed from the surrounding tissue. Small patches (≈ 4 mm^2) of the whole aorta were attached en face on Cell-Tak (BD Biosciences, Bedford, MA) coated glass, making it accessible for further experiments. After preparation, the patches were cultured in minimal essential medium (Invitrogen Corp., La Jolla, CA) supplemented with 10% fetal calf serum (PAA Laboratories, Pasching, Austria), 1% minimal essential medium vitamins (Invitrogen), 1% minimal essential medium nonessential amino acids (Invitrogen), and 1% penicillin/streptomycin (100 U/mL/100 mg/mL). Preservation of the EC layer on aorta preparations was confirmed by immunostaining of platelet endothelial cell adhesion molecule 1 (data not shown), and individual ECs on those preparations were studied.

Tissue Preparation of Mouse Heart/Damage Score Analysis of the Infarct or Scar Size

Preparation of the mouse hearts for histologic analyses was performed as described previously.[37] Five animals per group, evaluating at least 10 sections per heart, were included in the statistical analysis. Mice were sacrificed 9 days after MI; hearts were harvested and cut into sections (5 μm thick) below the ligation suture. Tissues were fixated, embedded in paraffin, and stained with hematoxylin and eosin for histologic evaluation of tissue damage.

Fixation and Preparation

For fixation, the hearts were cut in half, then put into 4% paraformaldehyde for 24 hours at room temperature and in 0.4% paraformaldehyde for another 24-hour period. After draining the tissue using a Leica TP1020 Automatic Tissue Processor (Leica Biosystems, Wetzlar, Germany), the organs were embedded in pure paraffin (CN49.2; Carl Roth GmbH + Co KG, Karlsruhe, Germany) overnight. Paraffin blocks were cooled with a Leica EG1130 Cold Plate for cooling the embedding molds and paraffin blocks and cut using a Microm HM440E microtome (all: Leica

Biosystems). Sections were made in 5-μm steps through the whole organ and processed at regular intervals of 500 μm (resulting in a total of 10 to 13 sections per heart).

Hematoxylin and Eosin Staining

For the hematoxylin and eosin staining, all materials and prepared reagents were equilibrated to room temperature before use. The sections were deparaffinized and hydrated in distilled water. Afterwards, the hematoxylin (T865.29; Carl Roth GmbH + Co KG) was applied to completely cover the tissue sections and incubated for 7 minutes. Slides were rinsed for 10 to 15 minutes to remove excess stain and bluing from the tissue sections. The eosin solution (X883.2; Carl Roth GmbH + Co KG) was then added, completely covering the tissue for 1 minute, and rinsed again in two changes of distilled water. After that, the slides were dipped in absolute alcohol to dehydrate them and mounted in rapid nonaqueous mounting medium (Entellan; 1.079.610.100; Merck Chemicals, Darmstadt, Germany).

Microscopy

Images were captured under a Keyence microscope (Keyence Corp.) at a ×60 magnification using the BZ Viewer software version 2.2 (Keyence Corp.) and processed using the BZ Analyzer-II software version 2.2 (Keyence Corp.). The infarcted area was measured by planimetry using ImageJ software version 1.52a. In all, 10 to 13 sections from different areas of each heart were evaluated. Areas of the infarction zone were measured and recorded in micrometers squared. The scar was defined as the region between the living myocytes and the cardiac membrane. The infarction size for each section was calculated as a ratio of the infarcted segment (MI area)/the total left ventricular segment (LV area): LV infarction (percentage). Values are means ± SD. The infarct sizes resulting from ligatures were compared using analysis of variance with *post hoc* comparisons. Observers were single blinded to the experimental protocol.

Damage Score

A damage score was used for quantitative estimation of tissue damage (compare with Zingarelli et al[38]: score of 0, no damage; 1, mild damage: interstitial edema and focal necrosis; 2, moderate damage: diffuse myocardial cell swelling and necrosis; 3, severe damage: necrosis with the presence of contraction bands and neutrophil infiltrate; and 4, highly severe damage: widespread necrosis with the presence of contraction bands, neutrophil infiltrate, and hemorrhage).

Statistical Analysis

Data were analyzed using IBM SPSS Statistics for Windows version 27.0 (IBM Corp., Armonk, NY), and the two-dimensional graphic and biostatistics software GraphPad Prism version 7 (GraphPad Software Inc., La Jolla, CA) was used to prepare the figures. Gaussian distribution was determined by D'Agostino and Pearson omnibus normality test. Data were tested for outliers before applying statistical tests using the ROUT outlier test based on the false discovery rate (Q value = 1%). Outliers were omitted from further analysis.

Differences between two groups were analyzed using *t*-test for parametric values or the Wilcoxon−*U*-test for nonparametric values, followed by *post hoc* analysis. Differences between three or more groups were analyzed using one-way analysis of variance with Bonferroni correction for multiple comparisons for parametric values or the Kruskal-Wallis test by ranks for nonparametric values, followed by *post hoc* analysis. For linear regression, Pearson correlations (r) were used. Differences were considered statistically significant when $P < 0.05$ ($^{*}P < 0.05$, $^{**}P < 0.01$, $^{***}P < 0.001$, and $^{****}P < 0.0001$). Data are presented as absolute values of means ± SD.

Results

Syndecan-1 Treatment Improves eGC and CTX after Enzymatic Degradation with Heparinase-I

The effects of treatment with rSyn-1 on the nanomechanical properties of the endothelial surface layers (eGC and CTX) were first studied *in vitro* in HUVECs. HUVECs were treated with Hep-I (0.1 U/μL for 60 minutes), as described previously,[36] to shed eGC components and allowed to recover for 24 hours in either the presence or the absence of rSyn-1. The nanomechanical properties (height and stiffness) were probed using the AFM nanoindentation technique.

The mechanical properties of eGC and CTX changed after treatment with Hep-I: Hep-I reduced eGC height by 61% compared with CTR (Figure 1A) (mean ± SD: 178 ± 36 versus 69 ± 5 nm; $P < 0.0001$). After 24 hours of recovery without rSyn-1, eGC height was not statistically significantly restored compared with the Hep-I group. In contrast, recovery combined with rSyn-1 treatment fully restored the eGC height compared with the CTR group (Figure 1A).

Hep-I−mediated shedding of eGC led to the softening of eGC by 30% compared with CTR (Figure 1B) (0.41 ± 0.07 versus 0.29 ± 0.04 pN/nm; $P < 0.001$), as shown previously.[36] Spontaneous restoration after 24 hours was not observed. Treatment with rSyn-1 increased eGC stiffness by 26% compared with that of Hep-I, and reached control levels (Figure 1B).

The enzymatic degradation of the eGC with Hep-I also influenced the mechanical properties of the CTX. Hep-I treatment increased cortical stiffness by 18% compared with treatment with CTR (Figure 1C) (1.25 ± 0.02 versus 1.05 ± 0.09 pN/nm; $P < 0.0001$). Spontaneous restoration did not occur after 24 hours; however, treatment with rSyn-1 led to softening of the CTX and full restoration to CTR levels (Figure 1C).

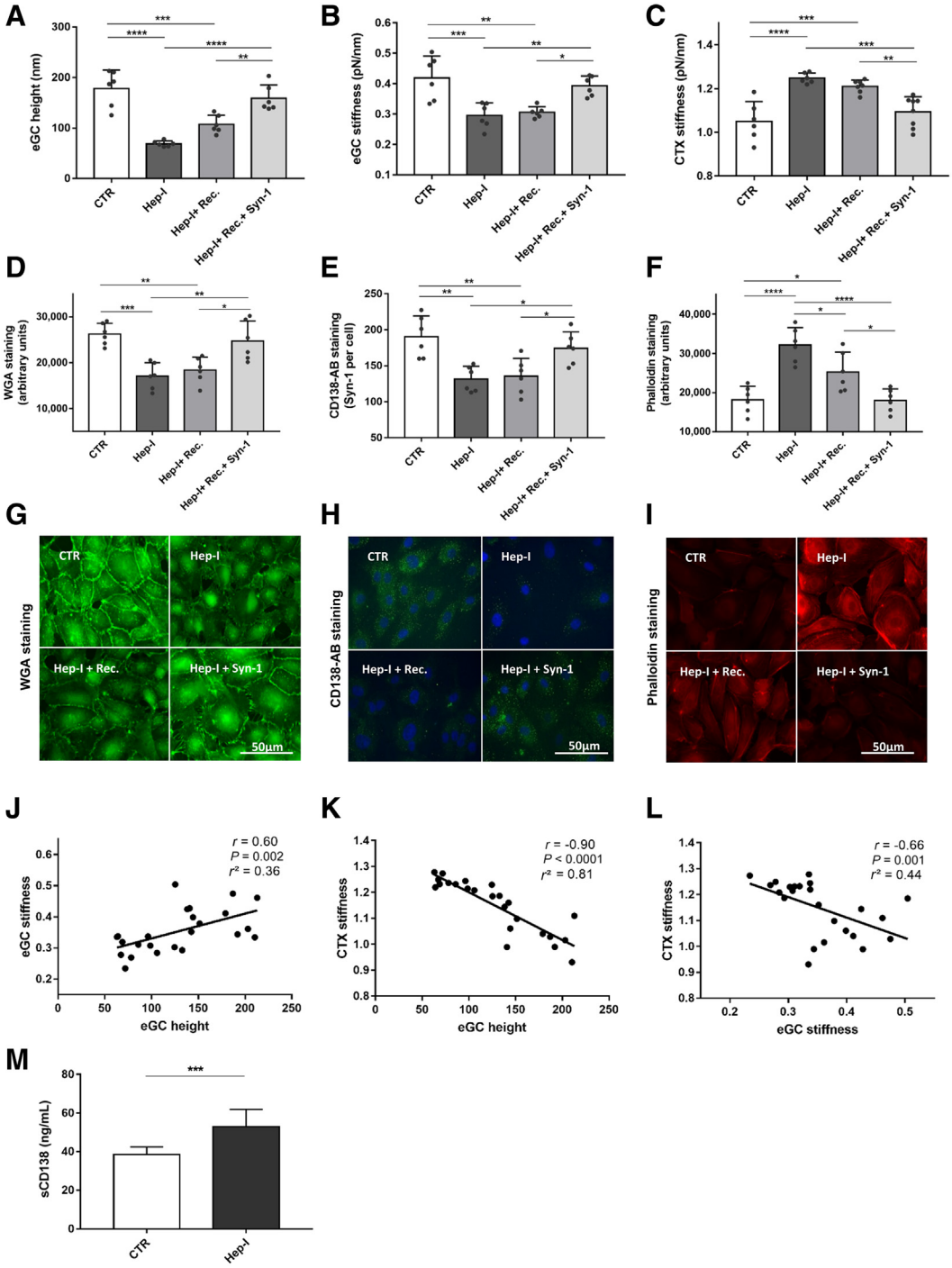

Figure 1 Syndecan-1 (Syn-1) treatment improves nanomechanics of endothelial glycocalyx (eGC) and cortex (CTX) after enzymatic degradation with heparinase-I (Hep-I). **A**–**C:** Histograms showing eGC height (**A**), eGC stiffness (**B**), and CTX stiffness (**C**) of human umbilical vein endothelial cell (HUVEC) monolayers measured via atomic force microscopy nanoindentation technique. Each dot represents the number of repetitions (each showing mean of 25 to 30 cells). **D**–**F:** Statistical analysis of fluorescence intensity differences after stimulation: wheat germ agglutinin (WGA)–stained (**D**), CD138 antibody (AB)–stained (**E**), and phalloidin– tetramethylrhodamine (TRITC)–stained (**F**) HUVEC monolayers. **G**–**I:** Representative fluorescence images and fluorescence intensity analyses of WGA-stained (**G**), CD138 antibody–stained (**H**), and phalloidin-TRITC–stained (**I**) HUVECs. **J**–**L:** Pearson correlation of eGC height versus eGC stiffness versus CTX stiffness after stimulation. **M:** Quantification of soluble syndecan-1 in culture medium after Hep-I treatment, measured via enzyme-linked immunosorbent assay. Groups: control (CTR), stimulation with cell culture media; Hep-I, stimulation with media + heparinase-I (0.1 U/µL for 60 minutes); Hep-I + recovery (Rec.), stimulation with heparinase-I (0.1 U/µL for 60 minutes) followed by 24 hours recovery time; Hep-I + Rec.+ Syn-1, stimulation with heparinase-I (0.1 U/µL for 60 minutes) followed by 24-hour recovery time + syndecan-1-treatment (8 pmol/L). Data are given as means ± SD (**A**–**F** and **M**). $N = 6$ (**A**–**F** and **M**). $^{*}P < 0.05$, $^{**}P < 0.01$, $^{***}P < 0.001$, and $^{****}P < 0.0001$ (one-way analysis of variance). Scale bars = 50 µm (**G**–**I**). sCD138, soluble CD138.

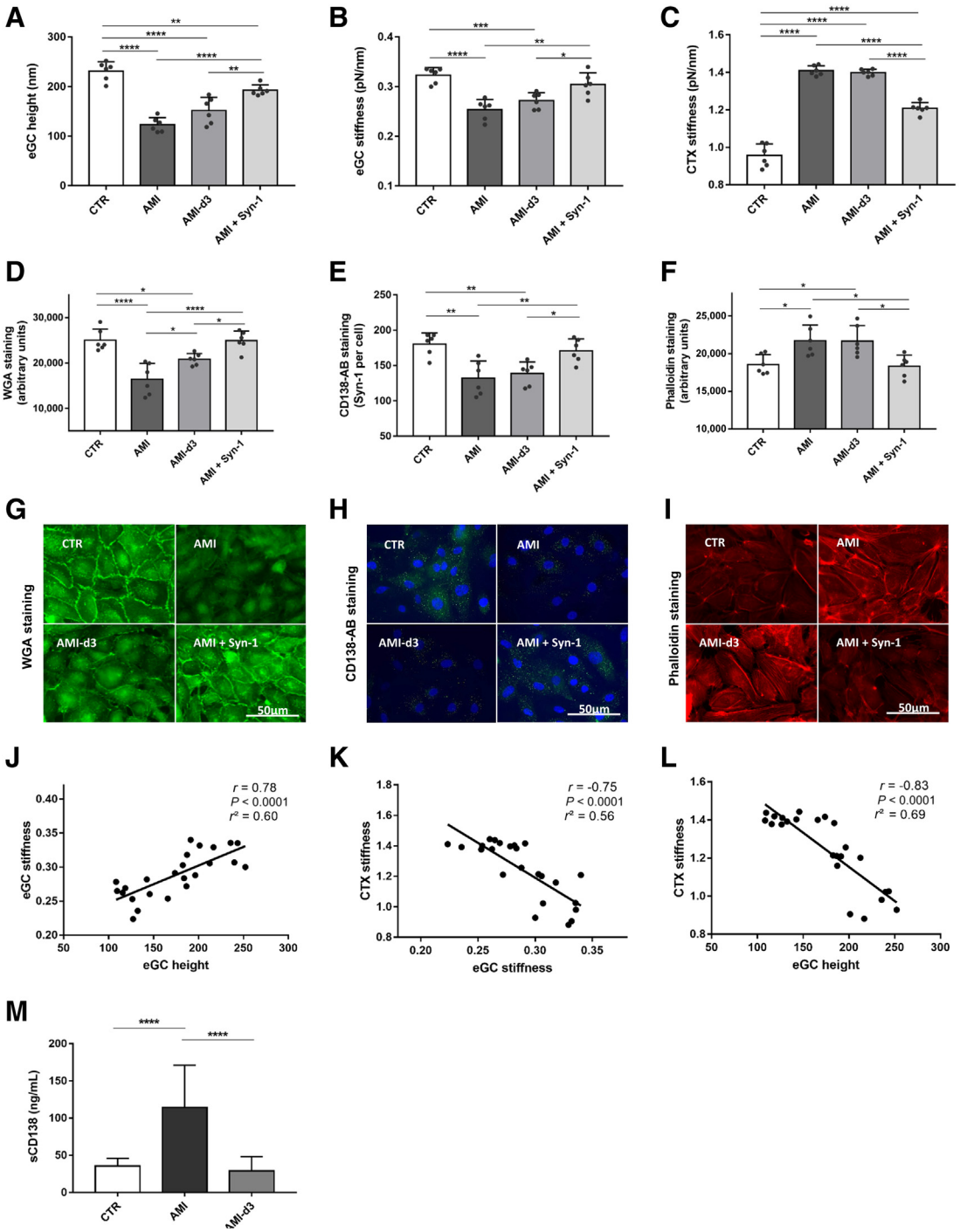

Figure 2 Syndecan-1 (Syn-1) treatment improves nanomechanics of endothelial cells after endothelial glycocalyx (eGC) shedding and cortex (CTX) stiffening in acute myocardial infarction (AMI). **A**–**C:** Histograms showing eGC height (**A**), eGC stiffness (**B**), and CTX stiffness (**C**) of human umbilical vein endothelial cell (HUVEC) monolayers measured via atomic force microscopy nanoindentation technique. Each dot represents the number of repetitions (each showing a mean of 25 to 30 cells). **D**–**F:** Statistical analysis of fluorescence intensity differences after stimulation: wheat germ agglutinin (WGA)–stained (**D**), CD138 antibody (AB)–stained (**E**), and phalloidin–tetramethylrhodamine (TRITC)–stained (**F**) HUVEC monolayers. **G**–**I:** Representative fluorescence images and fluorescence intensity analyses of WGA-stained (**G**), CD138 antibody–stained (**H**), and phalloidin-TRITC–-stained (**I**) HUVECs. **J**–**L:** Pearson correlation of eGC height versus eGC stiffness versus CTX stiffness after stimulation. **M:** Quantification of soluble syndecan-1 in culture medium after serum stimulation, measured via enzyme-linked immunosorbent assay. Groups: control (CTR), stimulation with cell culture media + 10% serum of healthy controls; AMI, stimulation with media + 10% serum of patients with ST-elevation myocardial infarction (STEMI); control 3 days after STEMI (AMI-d3), stimulation with media + 10% serum of patients with STEMI 3 days after myocardial infarction; AMI + Syn-1, stimulation with media + 10% serum of patients with STEMI + syndecan-1 (8 pmol/L). Data are given as means ± SD (**A**–**F** and **M**). $N = 6$ (**A**–**F** and **M**). $^{*}P < 0.05$, $^{**}P < 0.01$, $^{***}P < 0.001$, and $^{****}P < 0.0001$ (one-way analysis of variance). Scale bars = 50 µm (**G**–**I**). sCD138, soluble CD138.

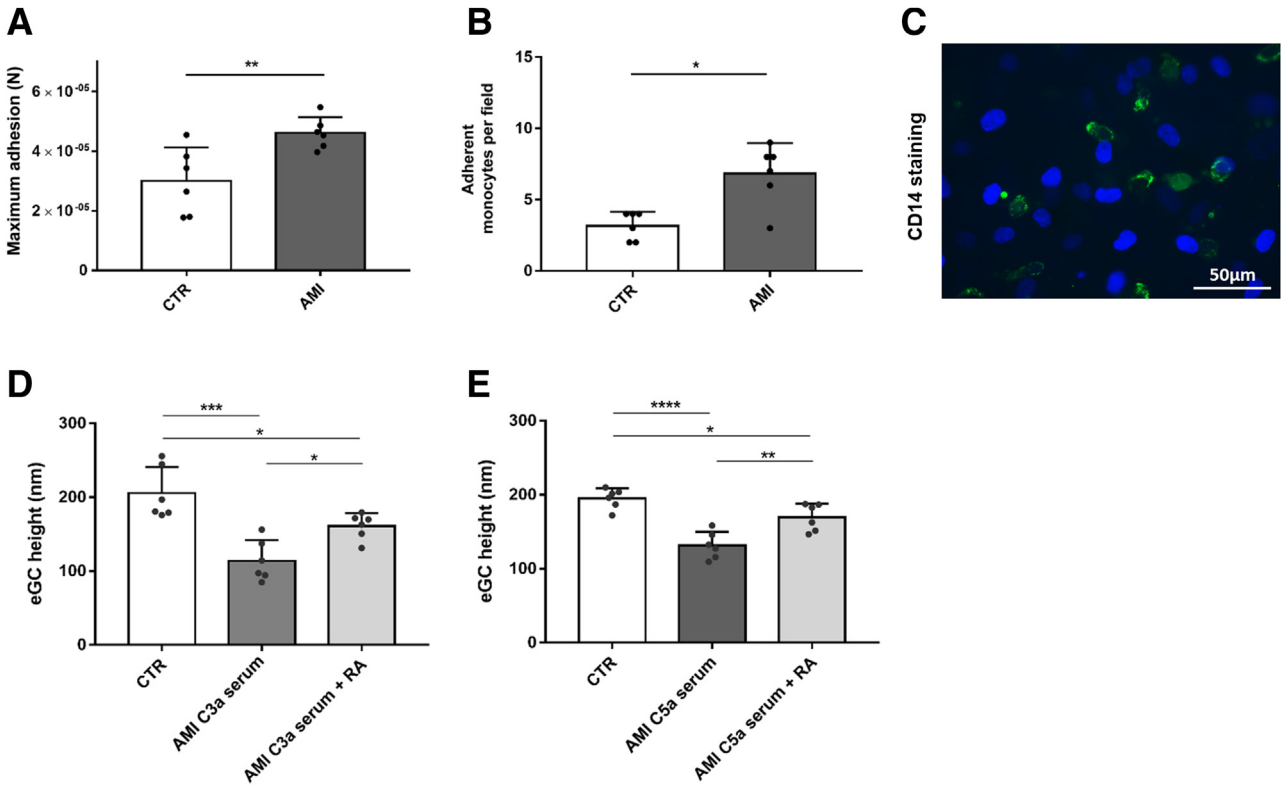

Figure 3 Monocyte adhesion increases during acute myocardial infarction (AMI), and anaphylatoxin C3a- and C5a-induced damage to endothelial glycocalyx (eGC) can be attenuated by specific anaphylatoxin receptor antagonists. **A:** Histograms showing maximum monocyte adhesion forces to human umbilical vein endothelial cell (HUVEC) monolayers, measured via atomic force microscopy (AFM) CellHesion technique. **B:** Adherent monocytes per field quantified via monocyte—wash-away assay and fluorescein isothiocyanate—labeled CD14 staining. Each dot represents the number of repetitions (each showing mean of 25 monocyte adhesion forces). **A** and **B:** The *t*-test was used. **C:** Representative fluorescence image of human monocytes (CD14-labeled monocytes; green) adhesive to HUVEC monolayer (HUVEC nuclei; blue). Stimulation with AMI serum led to increased monocyte adhesion forces and increased number of monocytes per field. Groups: control (CTR), stimulation with cell culture media + 10% serum of healthy control; AMI, stimulation with media + 10% serum of patients with ST-elevation myocardial infarction (STEMI). Data showing eGC height of HUVECs measured using the AFM nanoindentation technique. **D** and **E:** Stimulation with AMI serum containing high levels of C3a (**D**) and C5a (**E**) [measured via enzyme-linked immunosorbent assay (ELISA)] led to decreased eGC height. Specific receptor antagonism to C3a-receptor-1 (via SB 290157) and C5a-receptor-1 (via PMX53) attenuated eGC damage. **D** and **E:** One-way analysis of variance was used. Groups: CTR, stimulation with media + 10% serum of healthy control; AMI C3a serum, stimulation with media + 10% serum of patients with STEMI with high C3a concentration measured via ELISA; AMI C3a serum + receptor antagonist (RA), C3a receptor-antagonist SB 290157; AMI C5a serum, stimulation with media + 10% serum of patients with STEMI with high C5a concentration measured via ELISA; AMI C5a serum + RA, C5a receptor-antagonist PMX53. Data are given as means ± SD (**A**, **B**, **D**, and **E**). $N = 6$ (**A**, **B**, **D**, and **E**). $^{*}P < 0.05$, $^{**}P < 0.01$, $^{***}P < 0.001$, and $^{****}P < 0.0001$. Scale bar = 50 µm (**C**).

Results of the fluorescence staining were consistent with the AFM findings. The WGA staining revealed reduced fluorescence intensity of eGC after Hep-I treatment compared with that of CTR (Figure 1D) ($P < 0.001$). As in the AFM measurements, spontaneous eGC restoration did not occur. In contrast, rSyn-1 treatment induced equally robust fluorescence intensities, as observed in the CTR group, consistent with the full regeneration of eGC. Using the specific anti—Syn-1 antibody (anti-CD138), a reduction in Syn-1 immunofluorescence was demonstrated after enzymatic shedding with Hep-I (Figure 1E) ($P < 0.01$). Spontaneous restoration of the syndecans was not observed, whereas application of rSyn-1 increased the fluorescence intensity per cell up to control levels. In addition, the fluorescence staining of F-actin conformed with the results of the AFM-based measurements. The amount of F-actin after Hep-I treatment was 76% higher than in the CTR group (Figure 1F) ($P < 0.0001$), indicative of cortical stiffening. Application of rSyn-1 fully restored cortical F-actin levels compared with those of CTR (representative fluorescence staining is shown in Figure 1, G—I).

AFM parameters were interrelated: eGC height was positively associated with eGC stiffness ($r = 0.60$; $P = 0.002$) (Figure 1J), eGC height was negatively associated with CTX stiffness ($r = -0.90$; $P < 0.0001$) (Figure 1K), and eGC stiffness was negatively associated with cortical stiffness ($r = -0.66$; $P = 0.001$) (Figure 1L).

The ability of Hep-I to degrade eGC was confirmed by measuring the level of soluble Syn-1 (soluble CD138) using ELISA (Figure 1M). Soluble Syn-1 (soluble CD138) was significantly elevated after enzymatic treatment with Hep-I ($P < 0.001$).

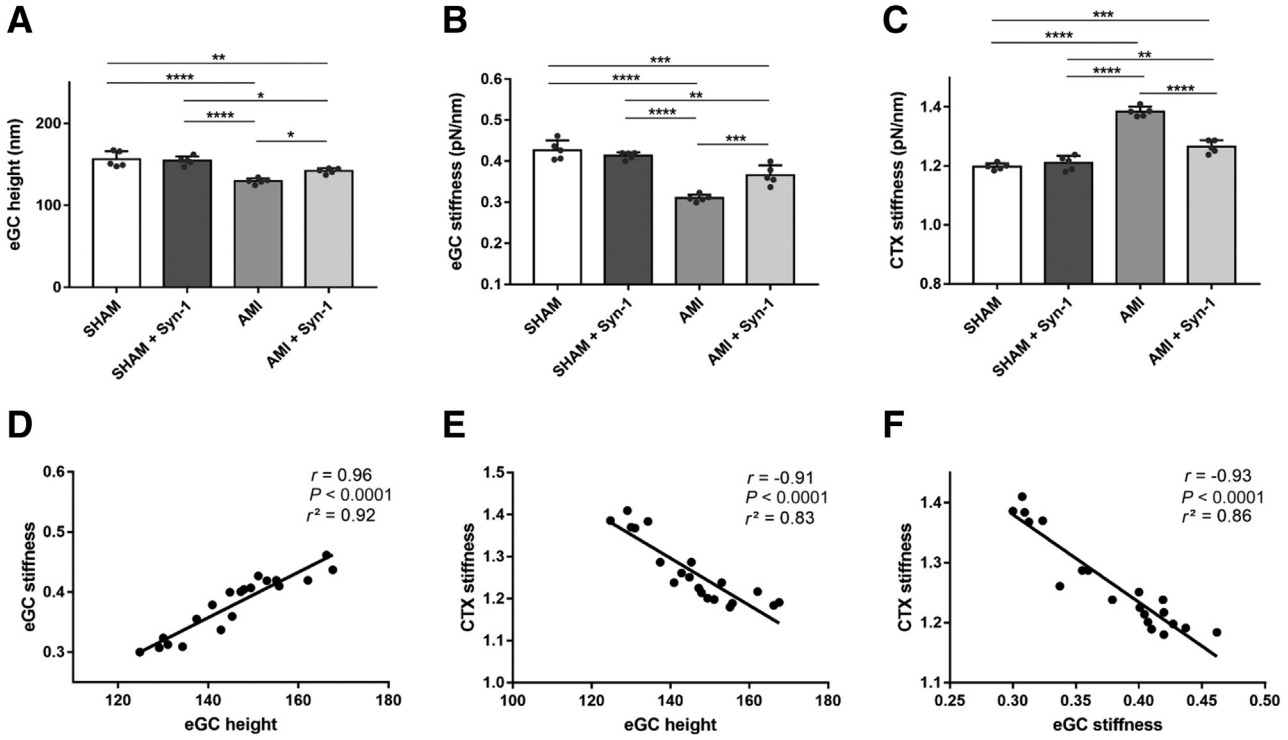

Figure 4 Syndecan-1 (Syn-1) treatment improves endothelial nanomechanics in a mouse model of myocardial infarction. **A**–**C:** Histograms showing endothelial glycocalyx (eGC) height (**A**), eGC stiffness (**B**), and cortex (CTX) stiffness (**C**) of living endothelial cells on isolated mouse aorta preparations measured using the atomic force microscopy nanoindentation technique. Each dot represents the number of repetitions (each showing a mean of 25 to 30 cells). **D**–**F:** Pearson correlation of eGC height versus eGC stiffness versus CTX stiffness after stimulation. Groups: sham-operated mice (SHAM), saline injection 24 hours before operation; SHAM + Syn-1, sham-operated mice with syndecan-1 treatment (4 μg/mouse; i.v. injection 24 hours before operation); acute myocardial infarction (AMI) mice, subjected to left coronary artery ligation to induce myocardial infarction (saline injection 24 hours before operation); AMI + Syn-1 mice, subjected to left coronary artery ligation to induce myocardial infarction with syndecan-1 treatment (4 μg/mouse; i.v. injection 24 hours before AMI). Data are given as means ± SD (**A**–**C**). $N = 5$ individual mice per group (**A**–**C**). $^{*}P < 0.05$, $^{**}P < 0.01$, $^{***}P < 0.001$, and $^{****}P < 0.0001$ (one-way analysis of variance).

Syndecan-1 Treatment Improves eGC and CTX in an *in Vitro* Model of AMI

Having demonstrated the efficacy of rSyn-1 in restoring HUVEC eGC after its enzymatic degradation, its performance following glycocalyx degradation by the human serum enriched in proinflammatory mediators was investigated next. To this end, serum samples derived from healthy control subjects and from patients with AMI on their first day of admission (AMI) as well as 3 days after AMI (AMI-d3) were employed; both time points are known to exhibit proinflammatory serum profiles.

AMI serum led to changes in the nanomechanical properties of eGC and CTX: AMI serum reduced the eGC height by 47% (Figure 2A) (CTR versus AMI: 231 ± 18 versus 123 ± 2 nm; $P < 0.0001$). In AMI-d3, the eGC remained damaged and eGC height was not restored (AMI versus AMI-d3). Those effects could be effectively prevented by rSyn-1 treatment (AMI + Syn-1: 192 ± 11 nm), which led to an increase in eGC height by 56% compared with AMI ($P < 0.0001$) and by 27% compared with AMI-d3 ($P < 0.01$). The stiffness of the eGC was affected by AMI serum (Figure 2B). After AMI stimulation, eGC stiffness was decreased by 21% compared with that in healthy controls (CTR versus AMI: 0.32 ± 0.02 versus 0.25 ± 0.02 pN/nm; $P < 0.0001$). No improvement in eGC height was detected after exposure to the AMI-d3 serum. The AMI serum-induced reduction observed in the height and softening of eGC was consistent with shedding of eGC components, which persisted for 3 days. Consistent with the cases of enzymatic degradation of eGC, rSyn-1 treatment combined with AMI serum fully restored levels to those of controls (AMI + Syn-1: 0.30 ± 0.02 pN/nm). After AMI, the cortical stiffness increased by 47% compared to that in healthy controls (Figure 2C) (CTR versus AMI: 0.96 ± 0.06 versus 1.41 ± 0.03 pN/nm; $P < 0.0001$). Treatment with rSyn-1 after exposure to AMI serum samples led to a softer cortex than in the AMI group, although CTR group levels were not reached (AMI versus AMI + Syn-1: 1.41 ± 0.03 versus 1.21 ± 0.03 pN/nm; $P < 0.0001$).

WGA staining (Figure 2D) was consistent with the AFM data and revealed a reduced fluorescence intensity of eGC components after treatment with AMI serum compared with that in the CTR group ($P < 0.0001$). In AMI-d3, however, spontaneous restoration of stained eGC components was observed compared with that in the AMI group ($P < 0.05$).

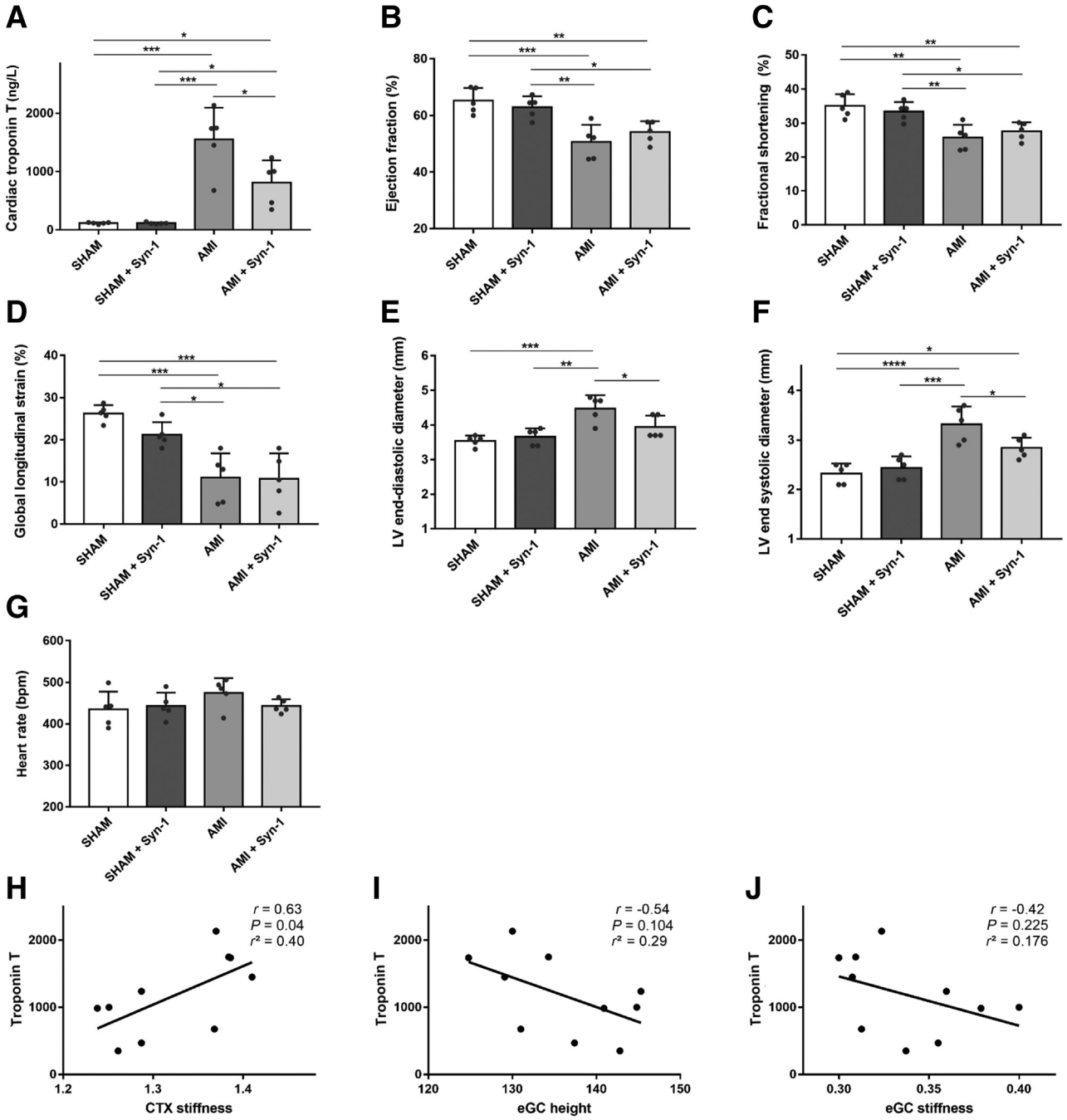

Figure 5 Cardiac troponin T and echocardiographic measurements in myocardial infarction mouse model. **A**–**G:** Histograms showing cardiac troponin T (**A**), as well as echocardiographic measurement data after acute myocardial infarction (AMI): ejection fraction (**B**), fractional shortening (**C**), global longitudinal strain (**D**), left ventricular (LV) end-diastolic diameter (**E**), LV end-systolic diameter (**F**), and heart rate (**G**). Each dot represents the number of repetitions. **H**–**J:** Pearson correlation of cardiac troponin T versus endothelial glycocalyx (eGC) height, eGC stiffness, and cortex (CTX) stiffness. Groups: sham-operated mice (SHAM), saline injection 24 hours before operation; SHAM + syndecan-1 (Syn-1), sham-operated mice with syndecan-1 treatment (4 μg/mouse; i.v. injection 24 hours before operation); AMI mice, subjected to left coronary artery ligation to induce myocardial infarction (saline injection 24 hours before operation); AMI + Syn-1 mice, subjected to left coronary artery ligation to induce myocardial infarction with syndecan-1 treatment (4 μg/mouse; i.v. injection 24 hours before AMI). Data are given as means ± SD (**A**–**G**). $N = 5$ individual mice per group (**A**–**G**). $^{*}P < 0.05$, $^{**}P < 0.01$, $^{***}P < 0.001$, and $^{****}P < 0.0001$ (one-way analysis of variance). bpm, beats per minute.

Consistent with AFM findings, the rSyn-1 treatment generated fluorescence intensities that were equally as robust as those in the CTR group, indicating a full regeneration of the eGC. Consistently, staining with specific anti–Syn-1 antibody (anti-CD138) (Figure 2E) indicated a reduction in Syn-1 after AMI compared with that in the healthy controls ($P < 0.01$), with no restoration detectable in AMI-d3. After rSyn-1 treatment, however, full restoration was detected.

Table 1 Echocardiographic Assessment after Myocardial Infarction in an *in Vivo* Mouse Model of Myocardial Infarction

Variable	SHAM, mean (SD)	SHAM + Syn-1, mean (SD)	AMI, mean (SD)	AMI + Syn-1, mean (SD)	*P* value (analysis of variance)
Ejection fraction, %	65.22 (4.55)	62.92 (3.88)	50.68 (6.07)	54.14 (3.84)	0.0004
Fractional shortening, %	35.06 (3.45)	33.38 (2.76)	25.74 (3.76)	27.6 (2.59)	0.0006
Global longitudinal strain, %	26.26 (1.94)	21.2 (2.96)	11 (5.79)	10.78 (6.01)	<0.0001
LV end-diastolic diameter, mm	3.54 (0.15)	3.66 (0.24)	4.48 (0.38)	3.94 (0.33)	0.0004
LV end-systolic diameter, mm	2.32 (0.20)	2.44 (0.23)	3.32 (0.36)	2.84 (0.21)	<0.0001
Heart rate, bpm	435 (42)	443 (31)	474 (36)	442 (16)	0.28

AMI, acute myocardial infarction; bpm, beats per minute; LV, left ventricular; SHAM, sham operation; Syn-1, syndecan-1.

The amount of cortical F-actin after AMI was higher than in the CTR group (Figure 2F) ($P < 0.05$), with no restoration 3 days after AMI. Adding rSyn-1 fully restored the cortical actin levels compared with those of the CTR group (representative fluorescence staining is shown in Figure 2, G–I).

AFM parameters were interrelated within the experimental groups: eGC height was positively associated with eGC stiffness ($r = 0.78$; $P < 0.0001$) (Figure 2J), eGC height was negatively associated with CTX stiffness ($r = -0.75$; $P < 0.0001$) (Figure 2K), and eGC stiffness was negatively associated with cortical stiffness ($r = -0.83$; $P < 0.0001$) (Figure 2L).

The level of soluble Syn-1 (soluble CD138) in patients with ST-elevation MI/AMI-d3, as well as control serum, as determined using ELISA (Figure 2M), showed that soluble Syn-1 was significantly elevated after AMI ($P < 0.0001$), whereas AMI-d3 and CTR groups showed no difference.

AMI Leads to Elevated Monocyte-Endothelium Interaction

To test whether the changes in eGC conformation have a functional impact on ECs, monocyte-endothelium interaction experiments were performed using a qualitative (CellHesion technique) as well as a quantitative (wash-away assay) approach.

The AFM-based CellHesion technique demonstrated elevated adhesion forces between human monocytes and endothelial monolayers after AMI stimulation (Figure 3A) ($P < 0.0001$). In the monocyte wash-away assay, the number of adherent monocytes per field was increased by 42% after AMI (Figure 3B) ($P < 0.0001$). Figure 3C shows a representative image of the CD14 staining.

Anaphylatoxin C3a- and C5a-Induced Damage of the eGC Can Be Attenuated by Specific Anaphylatoxin Receptor Antagonists

The concentrations of anaphylatoxins C3a and C5a in patient serum samples were quantified by using ELISA (C3a mean: 1233 ng/mL; C5a mean: 79 ng/mL). HUVECs were exposed to AMI serum samples with elevated levels of anaphylatoxins, as described above.

AMI serum with elevated C3a levels reduced eGC height by 44% (Figure 3D); serum with elevated C5a caused a reduction of 32% (Figure 3E) compared with that in the controls (both $P < 0.05$). Specific receptor antagonism to C3a-receptor-1 (via SB 290157) or to C5a-receptor-1 (via PMX53) attenuated the eGC damage (C3a: $P < 0.05$; C5a: $P < 0.01$) (Figure 3, D and E).

Syndecan-1 Treatment Improves eGC and CTX in an *ex Vivo* Mouse Model of MI

Encouraged by the aforementioned *in vitro* findings, whether similar therapeutic efficacy can be achieved *in vivo* was explored next. Therefore, effects of rSyn-1 were further tested in a mouse model of MI. Mice were subjected to sham operation (SHAM) or left coronary artery ligation to induce AMI, with or without rSyn-1 treatment via i.v. injection. *Ex vivo* studies performed in mouse aorta examined the height and stiffness of eGC as well as CTX stiffness of ECs probed using the AFM nanoindentation technique.

Neither eGC nor CTX nanomechanics quantified in the SHAM control group differed from SHAM with rSyn-1, indicating that intact and functional endothelial surfaces in these vessels could not be affected by treatment with rSyn-1 (Figure 4, A–C). In contrast, after AMI, eGC height and eGC stiffness (Figure 4A) were reduced by 17% (SHAM versus AMI: 156 ± 10 versus 130 ± 4 nm; $P < 0.0001$) and by 27% (SHAM versus AMI: 0.43 ± 0.02 versus 0.31 ± 0.01 pN/nm; $P < 0.0001$), respectively, compared with SHAM. Those effects could be prevented by rSyn-1 treatment (10% eGC height, AMI versus AMI + Syn-1: 130 ± 4 versus 142 ± 3 nm; $P < 0.05$). Similarly, eGC stiffness (Figure 4B) was increased after rSyn-1 treatment by 17% compared with AMI (0.31 ± 0.01 versus 0.37 ± 0.02 pN/nm; $P < 0.001$).

In Figure 4C, an increased CTX stiffness by 15% in the AMI group is shown compared with sham-operated mice (SHAM versus AMI: 1.2 ± 0.11 versus 1.38 ± 0.01 pN/nm; $P < 0.0001$). rSyn-1 treatment induced CTX softening compared with no treatment by 9% (1.38 ± 0.01 versus 1.27 ± 0.02 pN/nm; $P < 0.0001$). Although rSyn-1 treatment led to an improvement in both eGC and CTX, levels of sham-operated animals were not reached.

AFM parameters were interrelated within the experimental groups. eGC height was positively associated with

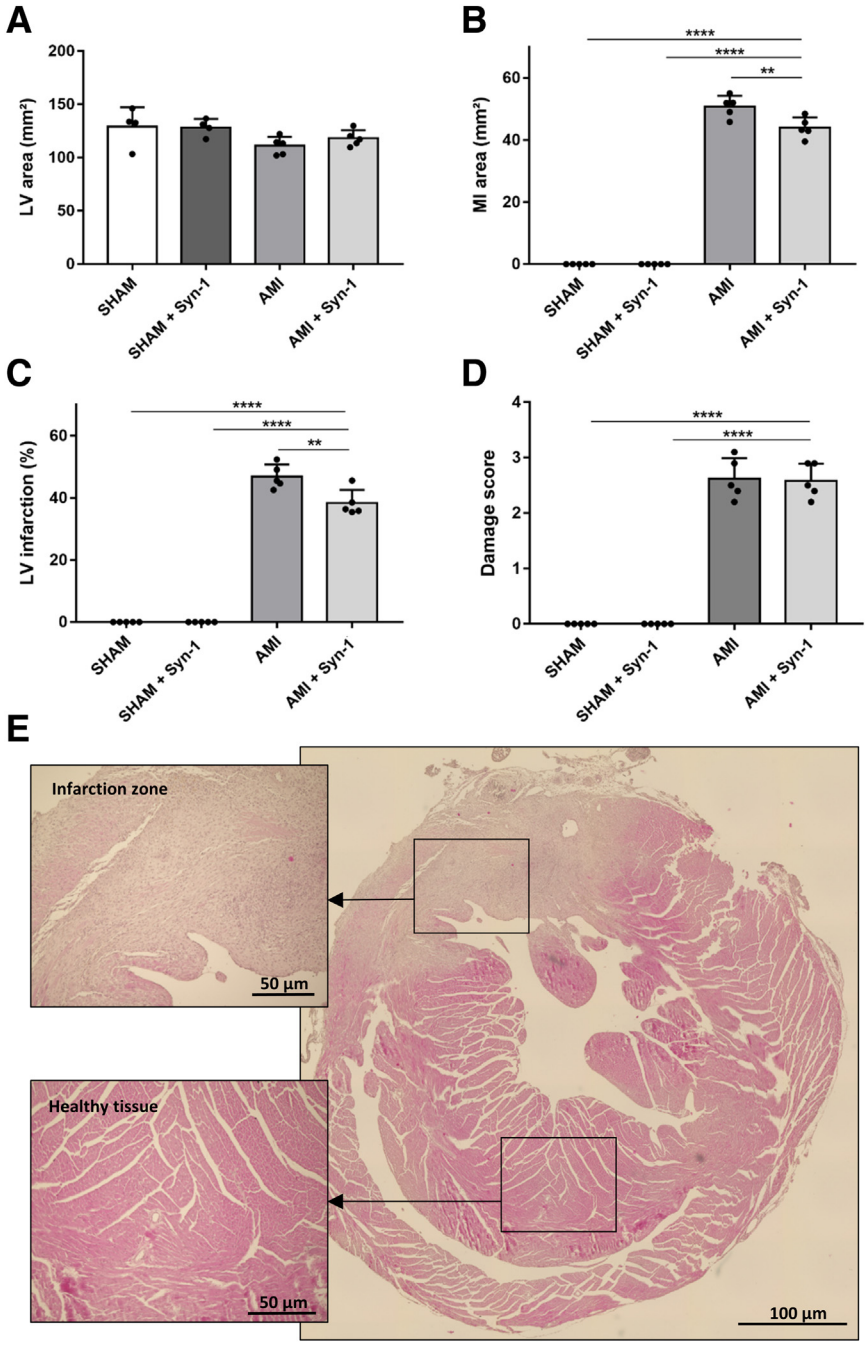

Figure 6 Histologic assessment of infarcted myocardium. Data showing histologic evaluation of myocardial damage after acute myocardial infarction (AMI). **A**–**C:** Areas measured in square millimeters of left ventricular (LV) area (**A**), myocardial infarction (MI) area (**B**), and LV/MI ratio (**C**). **D:** Myocardial damage score: 0 indicates no damage; 1, interstitial edema and focal necrosis; 2, diffuse myocardial cell swelling and necrosis; 3, necrosis with the presence of contraction bands and neutrophil infiltrate; and 4, widespread necrosis with the presence of contraction bands, neutrophil infiltrate, and hemorrhage (scored according to the method described by Zingarelli et al[38]). Each dot represents the number of repetitions. **E:** Representative hematoxylin and eosin staining of infarcted myocardium showing infarction zone versus healthy tissue. Groups: sham-operated mice (SHAM), saline injection 24 hours before operation; SHAM + syndecan-1 (Syn-1), sham-operated mice with syndecan-1 treatment (4 μg/mouse; i.v. injection 24 hours before operation); AMI mice, subjected to left coronary artery ligation to induce myocardial infarction (saline injection 24 hours before operation); AMI + Syn-1 mice, subjected to left coronary artery ligation to induce myocardial infarction with syndecan-1 treatment (4 μg/mouse; i.v. injection 24 hours before AMI). Data are given as means ± SD (**A**–**D**). $N = 5$ individual mice per group (**A**–**D**). Scale bars: 50 μm (infarction zone and healthy tissue; **E**); 100 μm (overview shot; **E**). $^{**}P < 0.01$, $^{****}P < 0.0001$ (one-way analysis of variance).

eGC stiffness ($r = 0.96$; $P < 0.0001$) (Figure 4D), eGC height was negatively associated with CTX stiffness ($r = -0.91$; $P < 0.0001$) (Figure 4E), and eGC stiffness was negatively associated with cortical stiffness ($r = -0.91$; $P < 0.0001$) (Figure 4F).

Troponin T Levels and Echocardiographic Assessment after Inducing MI in an *in Vivo* Mouse Model of MI

In parallel with the assessment of the nanomechanical properties of aortic endothelial eGC and CTX *ex vivo*, echocardiographic data and cardiac troponin T levels were determined in AMI mice *in vivo*.

Troponin T levels in the sham groups were within the standard range (Figure 5A), but were significantly elevated in the AMI mice. rSyn-1 treatment after inducing AMI significantly reduced troponin T levels (by 48%) compared with those in the AMI group, indicating less cardiomyocyte damage (AMI versus AMI + Syn-1: 1550 ± 543 versus 809 ± 380 ng/L; $P < 0.05$).

The echocardiographic assessment, including ejection fraction, fractional shortening, global longitudinal strain, LV

end-diastolic diameter, LV end-systolic diameter, and heart rate, is summarized in Table 1. All measured parameters, except for heart rate, showed significant differences between sham-operated and AMI groups.

rSyn-1 treatment had no effect on the echocardiographic parameters of sham-operated mice. AMI, however, led to a reduction in ejection fraction (65.22% versus 50.68%) (Figure 5B), fractional shortening (35.06% versus 25.74%) (Figure 5C), and global longitudinal strain (26.26% versus 11.0%) (Figure 5D) compared with that in the sham-operated mice. AMI was also associated with an increase in left ventricular end-diastolic diameter (SHAM versus AMI: 3.54 ± 0.15 versus 4.48 ± 0.38 mm) (Figure 5E) and left ventricular end-systolic diameter (SHAM versus AMI: 2.32 ± 0.20 versus 3.32 ± 0.36 mm) (Figure 5F) compared with that in sham-operated mice. These findings suggest an overall reduction in cardiac function after AMI.

Notably, treatment with rSyn-1 improved both left ventricular end-diastolic diameters ($P < 0.05$) (Figure 5E) and left ventricular end-systolic diameter ($P < 0.05$) (Figure 5F) compared with the AMI group without treatment. Heart rate was unchanged throughout the study groups (Figure 5G).

AFM measurements of eGC and CTX nanomechanic properties were correlated with cardiac troponin T within the MI groups. CTX stiffness positively correlated with troponin T ($r = 0.63$; $P = 0.04$) (Figure 5H), whereas eGC height (Figure 5I) and eGC stiffness (Figure 5J) were not correlated.

Histologic Assessment of Infarcted Mouse Hearts

Histologic analyses were conducted to detect the level of cardiac damage in AMI mice. Assessment of hematoxylin and eosin staining of the mouse hearts showed no difference in the average LV area (Figure 6A). Histologic examination of the infarcted hearts revealed that rSyn-1 treatment could not prevent marked necrosis and advanced fibrotic conversion of the cardiac tissue. Sham-operated hearts had healthy cardiac tissue.

rSyn-1 treatment after inducing AMI reduced the MI area by 9% compared with that in the untreated AMI mice (AMI versus AMI + Syn-1: 50.76 ± 8.9 versus 45.96 ± 8.44 mm^2; $P < 0.01$) (Figure 6B). In addition, the MI left ventricular ratio (LV infarction) (Figure 6C) was diminished by 6% after rSyn-1 treatment (AMI versus AMI + Syn-1: 46.84% versus 40.33%; $P < 0.01$). This reduction in infarct size after rSyn-1 treatment matches the improved levels of cardiac troponin T that were measured (Figure 5A). The degree of damage measured by using the damage score (scale of 0 to 4) revealed no significant difference between the AMI groups with or without rSyn-1 treatment (Figure 6D). Figure 6E shows a representative image of a hematoxylin and eosin−stained heart section.

Discussion

Recent studies indicate a need for new therapeutic strategies to prevent or repair damage of the eGC.[39] Especially in acute ischemic events, such as AMI, rapid restoration of the eGC may be decisive for the clinical outcome of the patients with AMI.[13] In this context, expeditious restoration of eGC integrity is advocated by Goligorsky and Sun[15] and Zhang et al,[40] who designed and synthesized a recombinant full-length Syn-1, containing its transmembrane and intracellular domain.

The mechanical properties of the endothelial surface layers (eGC and cortex) are known to be crucial for proper endothelial function, such as adequate response to shear stress,[20,41] and release of vasoactive substances, such as NO.[42] Structural damage of the eGC and chronic cortical actin web stiffening can thus be seen as early events of endothelial dysfunction, which culminate in chronic (cardio) vascular diseases.

The current study reports the impact of a full-length rSyn-1 in alleviating endothelial damage and accelerating the restoration of degraded eGC. To gain insights into the mechanism of AMI-dependent damage of the endothelial surface, *in vitro* experiments using primary ECs, such as a translational approach using patient serum samples, as well as *ex vivo* and *in vivo* experiments using a mouse model for MI, were employed. In the event of AMI, eGC components were being shed and the cortical stiffness increased both *in vitro* and *ex vivo*. Furthermore, the study showed that treatment with full-length rSyn-1 improved the nanomechanical properties of the eGC and the CTX, and rSyn-1 treatment partially ameliorated cardiomyocyte damage but did not lead to a functional improvement of the myocardium.

The reduction in height combined with a decreased stiffness of the eGC after enzymatic removal through Hep-I can be interpreted as shedding of eGC components.[18] The observed complete restoration of the eGC after additional treatment with rSyn-1 *in vitro* serves as a proof of principle that recombinant full-length Syn-1 is potentially efficacious in expediting restoration after eGC degradation, although components of the eGC other than Syn-1 are being shed during AMI.[5] In addition, Hep-I not only cleaved heparan sulfates, as predicted,[36] but also induced degradation of Syn-1 on ECs. At the translational level, the stimulation with serum samples obtained from patients with ST-elevation MI also induced shedding of the eGC and a traceable loss of Syn-1 on ECs. Notably, these findings could be confirmed *ex vivo* using ECs derived from aorta preparations in a mouse model of MI. The shedding of eGC during AMI might be caused by a variety of factors present in AMI serum[6] that are associated with cardiac mechanical stress, generalized vascular trauma, and an inflammatory response.[13] Those biomarkers and effectors of eGC degradation are elevated and activated during AMI, including

proinflammatory factors, such as ILs,[6] complement system,[7] catecholamines,[5] C-reactive protein,[8] and MMPs.[6] All these factors are known to facilitate degradation of Syn-1.[43] We, therefore, postulate that their presence in the AMI serum plays a key role in eGC impairment. MMPs, in particular, cleave the extracellular domains of syndecans.[44] Syn-1 is shed by MMP isoforms MMP-2, MMP-9, MMP-14, and a disintegrin and metalloprotease 17.[44] In AMI, the MMP-9 is up-regulated[45] and may be responsible for eGC impairment in AMI through cleaving of Syn-1. Furthermore, the complement system is activated during AMI, thus demonstrating an early marker of inflammation and tissue injury.[7] The complement anaphylatoxins C3a and C5a are important products of complement activation that may cause vascular damage and mediate hypertension, although the concrete mechanisms for this have not been clarified so far.[46,47] After stimulation with serum containing elevated levels of C3a and C5a, a shedding of eGC components was observed, which was prevented by applying specific receptor antagonists. Thus, the present data identify the eGC and its nanomechanical properties as an important target of anaphylatoxins and postulate that AMI-induced damage of the eGC is inter alia mediated by the C3a:C3aR or C5a:C5aR1 axes.

Although elevated circulating eGC components have previously been documented in AMI and cardiac interventions in experimental[48] and clinical settings,[49] the present data show, for the first time, the direct effects of AMI on the nanomechanical properties of the eGC and CTX of vascular ECs.

The integrity of the eGC plays an important role in endothelial function because of the close interaction between the eGC and the cellular cortex.[18] Endothelial function is defined by anti-thrombogenic and anti-inflammatory activity,[22] barrier function,[18] and contribution to blood pressure regulation.[16] In the present study, the impairment of endothelial function was demonstrated by measuring monocyte adhesion. During AMI, adhesion forces between monocytes and the endothelial surface were enhanced, showing proinflammatory changes in the endothelial surface. Quantitative as well as qualitative changes in monocyte adhesion indicate an unhealthy and dysfunctional endothelium. The present data are in agreement with previous studies showing that a shed eGC promotes the adhesion and pro-atherogenic effects of leukocytes.[35]

These attributes are influenced by the nanomechanical properties of the endothelium (stiffness and/or height), with NO being the key endothelium-derived smooth muscle–relaxing factor.[50] Synthesized by the endothelial nitric oxide synthase (nitric oxide synthase 3), NO diffuses to the adjacent smooth muscle cells and activates soluble guanylyl cyclase.[18] The increased cytosolic level of cGMP induces a decrease in intracellular calcium within the smooth muscle cells, which results in vasorelaxation.[18] Stiffness of the apical endothelial CTX represents a parameter that directly correlates with endothelial nitric oxide synthase function.[18,42] It has already been shown that pharmacologic softening of the CTX induced a higher NO release,[51] whereas CTX stiffening reduced endothelial nitric oxide synthase activity.[16,42] Thus, the degree of cortical stiffness directly correlates with the degree of endothelial NO release, demonstrating the link between nanomechanical properties of the ECs and their function.[18,23] A persistent stiffening of the CTX can, thus, be seen as dysfunctional.

In the present study, nanomechanical changes in the eGC correlated highly with nanomechanical changes in the CTX. Shedding of the eGC—and in particular, Syn-1—led to a stiffening of the CTX, indicating a dysfunctional endothelium, as stated above. Explanations of the underlying mechanism and the link between the shedding of the eGC and resulting cortical stiffening are embedded in the structure of Syn-1, composed of the ectodomain, the transmembrane, and the cytoplasmic domain.[43] The latter is directly associated with the actin cytoskeletal network via linker proteins, such as syntenin and synectin, which allows mechanotransduction from the cellular surface to intercellular junctions and throughout the cytoplasm.[43] In response, Syn-1 initiates cytoskeletal alignment and focal adhesion formation via activation of the GTPase Ras homolog family member A.[20] Among others, Syn-1 also regulates the activation of the phosphatidylinositol 3-kinase/Akt signaling pathway, mediating cellular activation of endothelial nitric oxide synthase and NO production.[18] The loss of Syn-1 or other eGC components impairs the EC responses to intraluminal stimuli, indicating endothelial dysfunction.[18,20] Indeed, after rSyn-1 treatment, not only were the nanomechanical properties of the eGC fully restored, but the nanomechanical properties of the CTX were also affected in this study, as shown by strong correlations in different experimental approaches in this study. This most likely indicates that rSyn-1 has been inserted into the plasma membrane, by virtue of its lipophilic transmembrane domain, and there is an association with the actin cytoskeletal network via its linker proteins. The present finding that rSyn-1 had no effect on eGC of intact cells endowed with dense endogenous glycocalyx, in contrast to the observed restoration of degraded glycocalyx (by heparinase or serum rich in proinflammatory mediators), argues in favor of this mechanism. The correlations between eGC integrity and CTX properties clearly show the functional link between the extracellular eGC and the intracellular CTX generated by the full-length rSyn-1 used in the experiments presented herein.

On the other hand, soluble Syn-1 has long been detected in the blood of patients with diverse diseases, such as inflammation, tumors, acute/chronic kidney disease, and cardiovascular diseases, including acute cardiogenic shock.[2,4,52,53] Soluble Syn-1 is predictive of survival in patients undergoing hemodialysis,[53] is associated with adverse clinical outcomes in acute cardiac events,[2,4] and is an independent predictor of short-term mortality in patients with acute heart failure,[2,4] amplifying the richness of information derived from the serum Syn-1 measurements.

Herein, Syn-1 likely originates not from a systemic source but rather from the endothelium itself.[13] The important difference in functionality between soluble Syn-1 and the rSyn-1 used in this study lies in the presence of its transmembrane and intracellular domains. As stated, these domains seem to be essential for implantation of Syn-1 and its connection to the actin cytoskeleton. To the best of our knowledge, the soluble Syn-1 detected in clinical trials after AMI treatment has never been sequenced. Whether this soluble Syn-1 contained the transmembrane and intracellular domains cannot be clarified at this point and would only be speculation. We postulate that the detectable soluble Syn-1 in AMI has been shed (broken), lacking a transmembrane and intracellular domain. Thus, soluble Syn-1 loses its ability to integrate into the cell membrane and to connect to the cortical actin. In contrast, the full-length rSyn-1 consists of the transmembrane domain and can thus be functionally inserted into the plasma membrane.

Present *in vivo* data on mouse myocardium suggest that rSyn-1 treatment potentially benefits cardiomyocyte outcome in AMI. Herein, structural differences between AMI and CTR groups could be determined: the amount of cardiac troponin T as well as the infarcted area—both reduced after rSyn-1-treatment—indicate a reduction in cardiomyocyte damage. Nevertheless, it must be emphasized that no significant differences in functional markers, including ejection fraction, fractional shortening, global longitudinal strain, and histologic damage score, detected via echocardiography, were found between the AMI group and treatment group. The link between preservation of the eGC and decreased cardiac remodeling may lie in post-MI inflammatory processes,[54] with inflammation playing a crucial role in acute ischemic cardiac injury and the contribution to postinfarction repair and remodeling.[54] Cells of the immune system have been shown to mediate both protective and damaging effects in heart remodeling.[55] Yet, the proinflammatory response and further damage are exacerbated in ischemic myocardium. Major contributors to this damage are infiltrating neutrophils, especially in the ischemic border zone, which produce and release reactive oxygen species, resulting in acute inflammation and cardiomyocyte apoptosis.[54] Because of its position on the vascular surface, the eGC acts as a firewall by mediating leukocyte-endothelium interactions[18] and modulating mechanisms of essential hypertension.[56] On intact eGC, leukocytes are tiptoeing with their cytoskeletal protrusions and barely come into contact with the adhesion molecules at the endothelial surface.[18] A compromised eGC barrier (ie, during AMI) may foster leukocyte adhesion and extravasation through interaction with L-selectin and chemokines.[57] Thus, intact eGC (ie, after treatment with rSyn-1) may be protective in the context of AMI and partly prevent cardiomyocyte damage by reducing inflammatory processes mediated by infiltrating leukocytes.

In conclusion, this study showed, for the first time, that preserving eGC has a protective effect on the cardiovascular system. With increasing prevalence of heart failure and IHD in overall aging populations, there is a need to develop diverse treatment methods.[52] Furthermore, the study also showed that eGC damage is mediated by the C3a:C3aR or C5a:C5aR1 axes, which will be further investigated in a follow-up project.

In this study, rSyn-1 was only used as a preventive treatment method right before AMI. Further investigations to evaluate the role of rSyn-1 as a potential post-AMI treatment method appear promising. The use of full-length rSyn-1 in this study focuses on prophylactic mechanisms to prevent eGC impairment and structural cardiomyocyte damage in AMI. However, a clear therapeutic effect of rSyn-1 after AMI could not be shown and requires further investigation.

Limitations of the Study

There are potential limitations to the interpretation of the data because of the limited number of serum samples used for the *in vitro* studies. The reason for these limitations relates to the fact that the AFM nanoindentation technique is time-consuming and sophisticated, which precludes analysis of considerably larger random sets of samples. The present experimental design ignores the potential influence of hemodynamic factors (eg, circulating fluid and shear stress). Another major limitation is the use of HUVECs and mouse aortal ECs, which limit extrapolating the rSyn-1 effects to other EC types (eg, coronary endothelial cells). Finally, syndecan-1 mRNA (or other glycocalyx proteoglycans) was not determined.

Nevertheless, the *in vivo* results of the present study have the potential to open new perspectives on the influence of rSyn-1 treatment on vascular endothelium and cardiomyocytes after AMI.

Acknowledgments

We thank all involved laboratory technicians of the University of Luebeck and University Magna Græcia as well as all involved clinicians of the Sana Kliniken Luebeck (heart catheter laboratory) for support of this study; and Sherryl Sundell for language editing.

Supplemental Data

Supplemental material for this article can be found at *http://doi.org/10.1016/j.ajpath.2022.12.009*.

References

1. Zahn R, Schweppe F, Zeymer U, Schiele R, Gitt AK, Mark B, Frilling B, Seidl K, Winkler R, Heer T, Schneider S, Senges J: Reperfusion therapy for acute ST-elevation and non ST-elevation myocardial infarction: what can be achieved in daily clinical

practice in unselected patients at an interventional center? Acute Card Care 2009, 11:92–98
2. Jung C, Fuernau G, Muench P, Desch S, Eitel I, Schuler G, Adams V, Figulla HR, Thiele H: Impairment of the endothelial glycocalyx in cardiogenic shock and its prognostic relevance. Shock 2015, 43: 450–455
3. Thiele H, Zahn R: Acute myocardial infarction-actual issues. Herz 2020, 45:507–508
4. Wernly B, Fuernau G, Masyuk M, Muessig JM, Pfeiler S, Bruno RR, Desch S, Muench P, Lichtenauer M, Kelm M, Adams V, Thiele H, Eitel I, Jung C: Syndecan-1 predicts outcome in patients with ST-segment elevation infarction independent from infarct-related myocardial injury. Sci Rep 2019, 9:18367
5. Ostrowski SR, Pedersen SH, Jensen JS, Mogelvang R, Johansson PI: Acute myocardial infarction is associated with endothelial glycocalyx and cell damage and a parallel increase in circulating catecholamines. Crit Care 2013, 17:R32
6. Wu Y, Pan N, An Y, Xu M, Tan L, Zhang L: Diagnostic and prognostic biomarkers for myocardial infarction. Front Cardiovasc Med 2021, 7:617277
7. Bavia L, Lidani KCF, Andrade FA, Sobrinho MIAH, Nisihara RM, de Messias-Reason IJ: Complement activation in acute myocardial infarction: an early marker of inflammation and tissue injury? Immunol Lett 2018, 200:18–25
8. Kusche-Vihrog K, Urbanova K, Blanqué A, Wilhelmi M, Schillers H, Kliche K, Pavenstädt H, Brand E, Oberleithner H: C-reactive protein makes human endothelium stiff and tight. Hypertension 2011, 57: 231–237
9. Puymirat E, Simon T, Cayla G, Cottin Y, Elbaz M, Coste P, Lemesle G, Motreff P, Popovic B, Khalife K, Labèque JN, Perret T, Le Ray C, Orion L, Jouve B, Blanchard D, Peycher P, Silvain J, Steg PG, Goldstein P, Guéret P, Belle L, Aissaoui N, Ferrières J, Schiele F, Danchin N; USIK, USIC 2000, and FAST-MI Investigators: Acute myocardial infarction: changes in patient characteristics, management, and 6-month outcomes over a period of 20 years in the FAST-MI program (French Registry of Acute ST-Elevation or Non-ST-Elevation Myocardial Infarction) 1995 to 2015. Circulation 2017, 136:1908–1919
10. Jung C, Ferrari M, Rödiger C, Fritzenwanger M, Goebel B, Lauten A, Pfeifer R, Figulla HR: Evaluation of the sublingual microcirculation in cardiogenic shock. Clin Hemorheol Microcirc 2009, 42:141–148
11. Alexander Y, Osto E, Schmidt-Trucksäss A, Shechter M, Trifunovic D, Duncker DJ, Aboyans V, Bäck M, Badimon L, Cosentino F, De Carlo M, Dorobantu M, Harrison DG, Guzik TJ, Hoefer I, Morris PD, Norata GD, Suades R, Taddei S, Vilahur G, Waltenberger J, Weber C, Wilkinson F, Bochaton-Piallat ML, Evans PC: Endothelial function in cardiovascular medicine: a consensus paper of the European Society of Cardiology Working Groups on Atherosclerosis and Vascular Biology, Aorta and Peripheral Vascular Diseases, Coronary Pathophysiology and Microcirculation, and Thrombosis. Cardiovasc Res 2021, 117:29–42
12. Adrie C, Adib-Conquy M, Laurent I, Monchi M, Vinsonneau C, Fitting C, Fraisse F, Dinh-Xuan AT, Carli P, Spaulding C, Dhainaut JF, Cavaillon JM: Successful cardiopulmonary resuscitation after cardiac arrest as a "sepsis-like" syndrome. Circulation 2002, 106:562–568
13. Abassi Z, Armaly Z, Heyman SN: Glycocalyx degradation in ischemia-reperfusion injury. Am J Pathol 2020, 190:752–767
14. Goligorsky MS: The cell "coat of many colors.". Am J Pathol 2020, 190:728–731
15. Goligorsky MS, Sun D: Glycocalyx in endotoxemia and sepsis. Am J Pathol 2020, 190:791–798
16. Oberleithner H, Callies C, Kusche-Vihrog K, Schillers H, Shahin V, Riethmüller C, Macgregor GA, de Wardener HE: Potassium softens vascular endothelium and increases nitric oxide release. Proc Natl Acad Sci U S A 2009, 106:2829–2834
17. Oberleithner H, Peters W, Kusche-Vihrog K, Korte S, Schillers H, Kliche K, Oberleithner K: Salt overload damages the glycocalyx sodium barrier of vascular endothelium. Pflugers Arch 2011, 462: 519–528
18. Fels J, Kusche-Vihrog K: Endothelial nanomechanics in the context of endothelial (dys)function and inflammation. Antioxid Redox Signal 2019, 30:945–959
19. Matyjaszczyk-Gwarda K, Kij A, Olkowicz M, Fels B, Kusche-Vihrog K, Walczak M, Chlopicki S: Simultaneous quantification of selected glycosaminoglycans by butanolysis-based derivatization and LC-SRM/MS analysis for assessing glycocalyx disruption in vitro and in vivo. Talanta 2022, 238(Pt 1):123008
20. Richter RP, Richter JR: Glycocalyx gone awry: pathologic cell signaling during endotheliopathy. Am J Biomed Sci Res 2019, 5:118
21. Tkachenko E, Rhodes JM, Simons M: Syndecans: new kids on the signaling block. Circ Res 2005, 96:488–500
22. Cosgun ZC, Fels B, Kusche-Vihrog K: Nanomechanics of the endothelial glycocalyx: from structure to function. Am J Pathol 2020, 190:732–741
23. Fels J, Jeggle P, Kusche-Vihrog K, Oberleithner H: Cortical actin nanodynamics determines nitric oxide release in vascular endothelium. PLoS One 2012, 7:e41520
24. Fels J, Jeggle P, Liashkovich I, Peters W, Oberleithner H: Nanomechanics of vascular endothelium. Cell Tissue Res 2014, 355: 727–737
25. Drüppel V, Kusche-Vihrog K, Grossmann C, Gekle M, Kasprzak B, Brand E, Pavenstädt H, Oberleithner H, Kliche K: Long-term application of the aldosterone antagonist spironolactone prevents stiff endothelial cell syndrome. FASEB J 2013, 27:3652–3659
26. Busche MN, Stahl GL: Role of the complement components C5 and C3a in a mouse model of myocardial ischemia and reperfusion injury. Ger Med Sci 2010, 8:Doc20
27. Bongoni AK, Lu B, McRae JL, Salvaris EJ, Toonen EJM, Vikstrom I, Baz Morelli A, Pearse MJ, Cowan PJ: Complement-mediated damage to the glycocalyx plays a role in renal ischemia-reperfusion injury in mice. Transplant Direct 2019, 5:e341
28. Brandwijk RJMGE, Michels MAHM, van Rossum M, de Nooijer AH, Nilsson PH, de Bruin WCC, Toonen EJM: Pitfalls in complement analysis: a systematic literature review of assessing complement activation. Front Immunol 2022, 13:1007102
29. Vicinanza C, Aquila I, Cianflone E, Scalise M, Marino F, Mancuso T, Fumagalli F, Giovannone ED, Cristiano F, Iaccino E, Marotta P, Torella A, Latini R, Agosti V, Veltri P, Urbanek K, Isidori AM, Saur D, Indolfi C, Nadal-Ginard B, Torella D: Kitcre knock-in mice fail to fate-map cardiac stem cells. Nature 2018, 555:E1–E5
30. Committee for the Update of the Guide for the Care and Use of Laboratory Animals; National Research Council: Guide for the Care and Use of Laboratory Animals. Eighth Edition. Washington, DC, National Academies Press, 2011
31. Cianflone E, Cappetta D, Mancuso T, Sabatino J, Marino F, Scalise M, Albanese M, Salatino A, Parrotta EI, Cuda G, De Angelis A, Berrino L, Rossi F, Nadal-Ginard B, Torella D, Urbanek K: Statins stimulate new myocyte formation after myocardial infarction by activating growth and differentiation of the endogenous cardiac stem cells. Int J Mol Sci 2020, 21:E7927
32. Aquila I, Cianflone E, Scalise M, Marino F, Mancuso T, Filardo A, Smith AJ, Cappetta D, De Angelis A, Urbanek K, Isidori AM, Torella M, Agosti V, Viglietto G, Nadal-Ginard B, Ellison-Hughes GM, Torella D: c-kit Haploinsufficiency impairs adult cardiac stem cell growth, myogenicity and myocardial regeneration. Cell Death Dis 2019, 10:436
33. Zatschler B, Dieterich P, Müller B, Kasper M, Rauen U, Deussen A: Improved vessel preservation after 4 days of cold storage: experimental study in rat arteries. J Vasc Surg 2009, 50:397–406
34. Jeggle P, Callies C, Tarjus A, Fassot C, Fels J, Oberleithner H, Jaisser F, Kusche-Vihrog K: Epithelial sodium channel stiffens the

vascular endothelium in vitro and in Liddle mice. Hypertension 2013, 61:1053−1059
35. Schierke F, Wyrwoll MJ, Wisdorf M, Niedzielski L, Maase M, Ruck T, Meuth SG, Kusche-Vihrog K: Nanomechanics of the endothelial glycocalyx contribute to Na+-induced vascular inflammation. Sci Rep 2017, 7:46476
36. Wiesinger A, Peters W, Chappell D, Kentrup D, Reuter S, Pavenstädt H, Oberleithner H, Kümpers P: Nanomechanics of the endothelial glycocalyx in experimental sepsis. PLoS One 2013, 8: e80905
37. Metzler B, Haubner B, Conci E, Voelkl J, Jehle J, Bauer M, Wolf D, Pachinger O, Xu Q: Myocardial ischaemia-reperfusion injury in haematopoietic cell-restricted beta1 integrin knockout mice. Exp Physiol 2008, 93:825−833
38. Zingarelli B, Salzman Andrew L, Szabó C: Genetic disruption of poly (ADP-ribose) synthetase inhibits the expression of P-selectin and intercellular adhesion molecule-1 in myocardial ischemia/reperfusion injury. Circ Res 1998, 83:85−94
39. Yilmaz O, Afsar B, Ortiz A, Kanbay M: The role of endothelial glycocalyx in health and disease. Clin Kidney J 2019, 12:611−619
40. Zhang X, Sun D, Song JW, Zullo J, Lipphardt M, Coneh-Gould L, Goligorsky MS: Endothelial cell dysfunction and glycocalyx - a vicious circle. Matrix Biol 2018, 71-72:421−431
41. Fronius M, Clauss WG: Mechano-sensitivity of ENaC: may the (shear) force be with you. Pflugers Arch 2008, 455:775−785
42. Fels J, Callies C, Kusche-Vihrog K, Oberleithner H: Nitric oxide release follows endothelial nanomechanics and not vice versa. Pflugers Arch 2010, 460:915−923
43. Stepp MA, Pal-Ghosh S, Tadvalkar G, Pajoohesh-Ganji A: Syndecan-1 and its expanding list of contacts. Adv Wound Care 2015, 4:235−249
44. Masola V, Zaza G, Arduini A, Onisto M, Gambaro G: Endothelial glycocalyx as a regulator of fibrotic processes. Int J Mol Sci 2021, 22: 2996
45. Chen Z, Yan Y, Wu J, Qi C, Liu J, Wang J: Expression level and diagnostic value of exosomal NEAT1/miR-204/MMP-9 in acute ST-segment elevation myocardial infarction. IUBMB Life 2020, 72: 2499−2507
46. Lillegard KE, Loeks-Johnson AC, Opacich JW, Peterson JM, Bauer AJ, Elmquist BJ, Regal RR, Gilbert JS, Regal JF: Differential effects of complement activation products c3a and c5a on cardiovascular function in hypertensive pregnant rats. J Pharmacol Exp Ther 2014, 351:344−351
47. Bhatia K, Ahmad S, Kindelin A, Ducruet AF: Complement C3a receptor-mediated vascular dysfunction: a complex interplay between aging and neurodegeneration. J Clin Invest 2021, 131: 144348
48. Lee SJ, Lee CK, Kang S, Park I, Kim YH, Kim SK, Hong SP, Bae H, He Y, Kubota Y, Koh GY: Angiopoietin-2 exacerbates cardiac hypoxia and inflammation after myocardial infarction. J Clin Invest 2018, 128:5018−5033
49. Bruegger D, Brettner F, Rossberg I, Nussbaum C, Kowalski C, Januszewska K, Becker BF, Chappell D: Acute degradation of the endothelial glycocalyx in infants undergoing cardiac surgical procedures. Ann Thorac Surg 2015, 99:926−931
50. Husain M, Moss J: Endothelium-dependent vascular smooth muscle control. J Clin Anesth 1988, 1:135−145
51. Peters W, Kusche-Vihrog K, Oberleithner H, Schillers H: Cystic fibrosis transmembrane conductance regulator is involved in polyphenol-induced swelling of the endothelial glycocalyx. Nanomedicine 2015, 11:1521−1530
52. Kim YH, Nijst P, Kiefer K, Tang WHW: Endothelial glycocalyx as biomarker for cardiovascular diseases: mechanistic and clinical implications. Curr Heart Fail Rep 2017, 14:117−126
53. Koch J, Idzerda NMA, Dam W, Assa S, Franssen CFM, van den Born J: Plasma syndecan-1 in hemodialysis patients associates with survival and lower markers of volume status. Am J Physiol Renal Physiol 2019, 316:F121−F127
54. Puhl SL, Steffens S: Neutrophils in post-myocardial infarction inflammation: damage vs. resolution? Front Cardiovasc Med 2019, 6:25
55. Kologrivova I, Shtatolkina M, Suslova T, Ryabov V: Cells of the immune system in cardiac remodeling: main players in resolution of inflammation and repair after myocardial infarction. Front Immunol 2021, 12:664457
56. Prat H, Araos P, Michea L: [Role of inflammation in hypertension]. Rev Med Chil 2021, 149:255−262
57. Celie JWAM, Beelen RHJ, van den Born J: Heparan sulfate proteoglycans in extravasation: assisting leukocyte guidance. Front Biosci (Landmark Ed) 2009, 14:4932−4949